Semi-Empirical Estimation of Strong Ground Motions During Large Earthquakes

AUTHOR(S):

IRIKURA, Kojiro

CITATION:

IRIKURA, Kojiro. Semi-Empirical Estimation of Strong Ground Motions During Large Earthquakes. Bulletin of the Disaster Prevention Research Institute 1983, 33(2): 63-104

ISSUE DATE:

1983-06

URL:

http://hdl.handle.net/2433/124917

Bull. Disas. Prev. Res. Inst., Kyoto Univ., Vol. 33, Part 2, No 298, June, 1983

Semi-Empirical Estimation of Strong Ground Motions During Large Earthquakes

By Kojiro IRIKURA

(Manuscript received March 22, 1983)

Abstract

A synthesis method is developed for estimating deterministically strong motions during the mainshock, using the records of small events such as foreshocks and aftershocks which occurred within the area of the mainshock fault. This synthesis formulation is based on the kinematic source model of Haskell type and the similarity law of earthquakes. The parameters for this synthesis are determined to be consistent with the scaling relations between the moments and the fault parameters such as fault length, width and dislocation rise time. If the ratio of the mainshock moment Mo to the small event one Mo_e is assumed to be N^3, then the mainshock fault can be divided into $N \times N$ elements, each dimension of which is consistent with that of the small event and N events at each element may be superposed with a specific time delay to correct the difference in the rise time between the mainshock and the small event and to keep a constant slip velocity between them. By means of this method, the mainshock velocity motions are synthesized using the small event records obtained by velocity-type-strong-motion-seismographs for 1980 Izu-Hanto-Toho-Oki Earthquake ($M=6.7$). The resultant synthesized motions show a good agreement with the observed ones in the frequency range lower than 1 Hz. Further, the synthesis formulation is improved to be applicable to the higher frequency motions, especially acceleration motions. This revised synthesis for the higher frequency motions is effective when we use the records from the small event having the fault length $L_e = V_r \cdot \tau$ (V_r: rupture velocity and τ: rise time of mainshock). The synthesized accelerograms by this revised method are in good agreement with the observed ones in the frequency range up to 5 Hz.

1. Introduction

The investigation of the synthesis of strong ground motions in the near field has significantly lagged, compared with that of long period motions in the far field. This is caused by the difficulties of theoretical treatment for high frequency motions included in the strong motions. The investigators for earthquake engineering have been concerned with the strong motions from the need of engineering. Therefore, the input motions usually used for the evaluation of earthquake resistant design criteria have been synthesized for some time, independently of the physical considerations of the earthquake source. Recently, seismologists have begun to take an active interest in strong motions to study the details of faulting, as strong motion data have been accumulating in the near field. On the other hand, many investigators concentrate their attention of engineering interest on reliable estimates of the strong

motions for earthquake resistant design of critical structures. The study of strong motions currently is one of the most remarkable subjects for seismology and earthquake engineering.

In this study, we have the purpose for engineering seismology to develop a reliable and practical synthesis method of strong motions, based on careful considerations of the physical properties of the earthquake fault.

The first successful attempt for theoretical calculation of strong motions was made by Aki (1968)[1] and Haskell (1969)[2], using kinematic source model, given by a propagating dislocation over a fault plane in an infinite homogeneous medium. Their source models are parameterized by five factors, fault length, fault width, rupture velocity, final offset of dislocation and rise time, which are essential for a deterministic fault model. Kawasaki et al. (1972)[3] gave exact expressions of seismic motions due to a double couple point source in a semi-infinite medium. Sato (1978)[4] proposed an approach to derive exact expressions of a series of 'rays' for layered media by applying the Cagniard-deHoop method, and Sato and Hirata (1980)[5] gave a new approach using integral evaluation to compute the seismic motions for layered media including the contributions from dispersive surface waves. Heaton and Helmberger (1979)[6] succeeded also in synthesizing strong motions on the basis of a generalized ray theory with the Cagniard-deHoop method for layered models. Bouchon (1979)[7] developed a method to compute strong motions for a propagating fault in layered media, based on a discrete wave number method. These synthesis methods calculating the strong motions based on a deterministic fault model have been successful in low frequency ranges (<1 Hz). At high frequencies these methods underestimate the strong motions, when a coherent rupture propagation is assumed. Indeterminable factors in the source and the propagating medium may strongly influence the high frequency ground motions. Hartzel and Helmberger (1982)[8] attempted to determine a localized area of larger dislocation, based on the analysis of some excellent set of records obtained in the 1979 Imperial Valley, California earthquake and the highly accurate calculation of the discrete wave number/finite element method (Alekseev and Mikkailenko, 1979)[9]. They proposed a more complex model with two localized sources better to explain the data.

A different approach to estimate strong motions is based on inhomogeneous fault models such as 〈barrier model〉 (Aki, 1979)[10] and 〈asperity model〉 (Macgarr, 1981)[11]. Barriers cause irregular distribution of slip during faulting and a consequence of this is an irregular distribution of stress drop. The numerical experiments performed by Das and Aki (1977)[12] and Mikumo and Miyatake (1978)[13] demonstrated clearly that barriers control the complexity of rupture and they are responsible for the generation of high frequency radiation. Papageorgiou and Aki (1981)[14] constructed an earthquake source model which provide a complete description of acceleration power spectra of direct body waves. They call it a specific barrier model. The fault surface is visualized as composed of an aggregate of circular cracks, and the strong motions are assumed to be generated by the stationary

occurrence of these localized ruptures as the rupture front propagates. Boatwright (1982)[15] constructed the same model for the far-field acceleration by combining the Madariaga (1977)[16] theory for the high-frequency radiation from crack models of faulting with a simple statistical source model. Based on these stochastic fault models, however, we cannot estimate deterministically the waveforms of the strong motions.

Another approach was proposed by Hartzell (1978)[17] to synthesize strong motions, utilizing observed seismograms from small events as Green functions. It is a most advantageous method because the Green functions include complex effects of the dynamical rupture process on the fault as well as heterogeneous structures around the source and an observation site, which are extremely cumbersome to evaluate. However, Hartzell's method has some problems which need to be improved. For example, in his method, the discrepancy between the dislocation rise time of a large event and that of a small event is not taken into account and the physical meaning of the scale factor Q is uncertain. Kanamori (1979)[18] and Hadley and Helmberger (1980)[19] attempted to predict the strong motions from large earthquakes applying Hartzell's method. In Japan, Irikura and Muramatu (1982)[20], Imagawa and Mikumo (1982)[21], and Iida and Hakuno (1982)[22] attempted to synthesize the mainshock motions using small shock motions such as foreshocks and aftershocks. Irikura and Muramatu, and Imagawa and Mikumo improved Hartzell's method by introducing the phase delayed summation with a specific time function to correct for the difference in the source time function between the mainshock and the small events. From the comparison with the observed seismograms of the mainshock, Irikura and Muramatu succeeded in the synthesis of strong motions lower than 1 Hz for 1980 Izu-Hanto-Toho-Oki Earthquake (M=6.7). On the other hand, Imagawa and Mikumo indicated that synthesized waveforms provide a satisfactory agreement to long-period components longer than 5 sec for the 1969 central Gifu Earthquake (M=6.6) and a stochastic fault model has to be introduced for shorter-period motions (T=1–2 sec), for example such as the variation of the rupture velocity on the fault plane.

In this study, a semi-empirical synthesis method for estimating the mainshock motions from records of small events has been formulated, based on the kinematic source model of Haskell type and the similarity law of earthquakes. The parameters for the synthesis are determined to be consistent with the scaling relations between moments and fault parameters such as fault length, width and dislocation rise time. The extent of validity and applicability of this synthesis method is discussed in two ways, (1) the numerical check of validity of the synthesis formulation, (2) the comparison between the synthesized mainshock motions and the observed ones.

As far as numerically calculated, we have found that smaller events are more preferable for utilization of the synthesis, because their source sizes approach a point as events are smaller and their records are suitable as Green functions for mainshock motions. However, accurate records from smaller events may be restricted to

a narrower and higher frequency range, because amplitudes at low frequencies become smaller than those of ground noises. In addition another problem has been reported. The scaling law of seismic spectra for smaller events shows some departure from the similarity assumption, which was studied to explain fairly well observations of earthquakes with magnitude greater than 6 (Aki, 1967[23], 1972[24], Kanamori and Anderson, 1975[25]). Thus, in order to synthesize large earthquake motions, we need to use records from small earthquakes larger than appropriate sizes. Then, we have to check the validity of the similarity relation between large and small earthquakes.

By means of the synthesis method in this study mainshock velocity motions are synthesized using the records from small earthquakes such as foreshocks and aftershocks obtained by the velocity-type-strong-motion-seismographs for the case of 1980 Izu-Hanto-Toho-Oki earthquake (the mainshock with $M=6.7$). The synthesized motions show a good agreement with the observed ones in the period range longer than 1 sec, that is, the rise time of the mainshock. The amplitudes of the synthesized motions tend to become smaller than those of the observed ones.

Further, the synthesis formulation has been improved to be applicable for shorter period motions, especially for strong acceleration motions, not statistically but deterministically. This revised method is based on an idea that the slips on the fault plane during the mainshock are able to be approximately replaced to the spatial distribution of the slips during small events. When we use the records from the small events having the fault length $L_e=V_r\cdot\tau$ (V_r, rupture velocity; τ, rise time of mainshock), we can synthesize effectively the mainshock motions without decreasing the amplitudes at the period range shorter than 1 sec. The synthesized accelerograms by means of this revised method show a good agreement with the observed accelerograms in the frequency range up to 5 Hz. This synthesis method implies the possibility of the prediction of strong ground motions for future large earthquakes using observed seismograms from small events which have occurred within or near the presumed fault area.

2. Relations between the Ground Motions from Large Events and Those from Small Events

2.1. Similarity of Earthquakes

The present estimation of strong motions from large earthquakes using the records from small events is based on the similarity assumption for earthquakes. We summarize here the similarity conditions between large and small events to prepare formulations for the synthesis of strong motions.

The similarity assumption was first introduced by Tsuboi[26] in the idea 'earthquake volume'. He derived that the total energy of an earthquake, E, is given by $E=\frac{1}{2}\mu(\Delta\varepsilon)^2V$, where μ is an effective elastic constant, $\Delta\varepsilon$ is an average strain drop and V is 'earthquake volume'. Assuming $L=3W$ (L: fault

length and W: fault width) together with the above relation, it results in a constant strain drop. Thus, earthquakes of different sizes are related by a one-parameter model. Aki (1967)[23] introduced a scaling law in which seismic spectrum grows with earthquake magnitude. He showed that the seismic spectra are scaled according to the fault length, assuming that the seismic moment is proportional to L^3 (L=fault length).

Furthermore, Kanamori and Anderson (1975)[25] and Geller (1976)[27] derived the following extended conditions of similarity:

$$L/W=\text{const.} \tag{1}$$
$$D/W=\text{const.} \tag{2}$$
$$L/(v_r\cdot\tau)=\text{const.} \tag{3}$$

where L and W are the length and the width of an earthquake fault, respectively, D, the final offset of the dislocation, τ, the rise time and v_r, the rupture velocity. These constants vary with the different nature of source type and different source region. These similarity conditions are derived as "averages" over a data set of 41 shallow earthquakes collected from all over the world, nevertheless, they fit observed data quite well. It may be very useful to relate the source parameters between the large and small events, if the ensemble of the events are classified according to the source regions and the source types. When two events with different size have occured within the same region, the following similarity relations are deduced from (1) to (3).

$$L/L_e=W/W_e=D/D_e=\tau/\tau_e=(Mo/Mo_e)^{1/3} \tag{4}$$

where the parameters without subscript are for a large event and those with subscript e, for a small one.

The important parameters neccessary for synthesis as well as the source geometry are rupture velocity v_r and rise time τ. Rupture velocities have been obtained and noted to have roughly a constant for earthquakes of different sizes. Geller (1976)[27] obtained the relation $v_r=0.72\beta$ as an average for reported rupture velocities.

The rise time τ is very difficult to determine since it involves assumptions on the fault model and is dependent on the rupture velocity. Geller obtained

$$\tau=16S^{1/2}/(7\pi^{3/2}\beta), \tag{5}$$

based on various theoretical assumptions and observational values of 14 earthquakes. Abe (1975)[28] reached a similar conclusion from a data set of five Japanese earthquakes. In the next section, using these similar conditions we will approach the synthesis of strong ground motions from small equarthquake motions.

2.2. Relation between the source-time-function of a large event and that of a small event

We consider a large event and a small event which occur within the same region

and have the same mechanism.

We call here the large event a mainshock and the small one an elementary earthquake. From the similarity conditions mentioned above, a relation is deduced between the source time functions of the mainshock and the elementary earthquake. A simple dislocation model of the Haskell type with a smooth coherent rupture propagation and a constant slip motion over a rectangutar fault (Haskell, 1964)[29] is useful to express this relation.

A schematic model is illustrated in **Fig. 1.** The far-field displacement $U_c(\boldsymbol{x}, t)$ at any point Q in an infinite homogeneous elastic medium due to dislocation $\Delta U(\xi, \eta, t)$ over the fault plane Σ can be written as

$$U_c(\boldsymbol{x}, t) = (R_c(\theta, \varphi)/4\pi\rho v_c^3 r) \cdot \mu \int_0^L \int_0^W \Delta \dot{U}(\xi, \eta, t - t_c) d\xi d\eta \tag{6}$$

where $t_c = r/v_c + \sqrt{\xi^2 + \eta^2}/v_r$,

μ is the rigidity, v_c is the wave velocity, r is the distance between the fault plane Σ and the point Q, R_c is the radiation coefficient, φ is the strike, θ is the dip angle, and subscript c indicates an appropriate wave type, P or SV or SH. The source time function $S(\boldsymbol{x}, t)$ associated only with source parameters is defined by a simple integral of the form,

$$S(\boldsymbol{x}, t) = \mu \int_0^L \int_0^W \Delta \dot{U}(\xi, \eta, t - t_c) d\xi d\eta. \tag{7}$$

Dividing the fault plane of the large event into $N_L \times N_W$, we take the dimension of

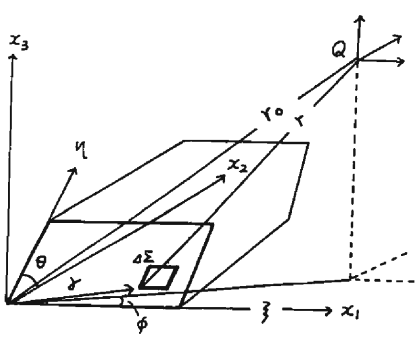

Fig. 1. Coordinate and fault plane geometry. The Haskell model of a rectangular fault is used.

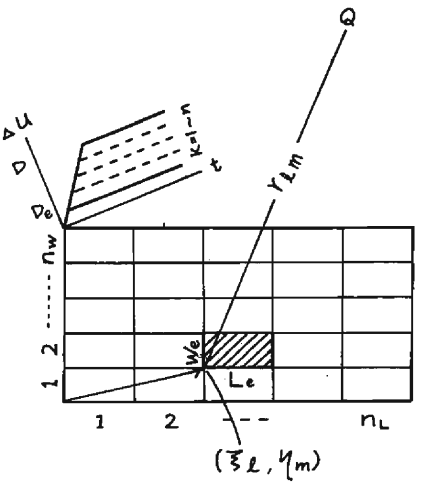

Fig. 2. Mainshock fault plane divided into $N_L \times N_W$ elements. An element corresponds to the fault dimension of a small event.

each element corresponding to that of the small event as shown by **Fig. 2.** The element has L_e in length and We in width. Equation (3) is rewritten in the following summation,

$$S(\boldsymbol{x}, t)=\sum_{l=1}^{N_L}\sum_{m=1}^{N_W}\mu\int_{\xi_l}^{\xi_l+L_e}\int_{\eta_m}^{\eta_m+W_e}\Delta\dot{U}(\xi_l, \eta_m, t-t_{c_{lm}})d\xi d\eta. \tag{8}$$

The dislocation function $\Delta U(\xi, \eta, t)$ at a point (ξ, η) on the fault plane Σ of the large event is taken to be a ramp function with a rise time τ and a final offset D. That is,

$$\begin{aligned}\Delta U(\xi, \eta, t)&=0 && t<0,\\ &=Dt/\tau && 0<t<\tau\\ &=D && t<\tau\end{aligned}$$

Similarly, the dislocation function $\Delta U_e(\xi, \eta, t)$ at the point (ξ, η) on the fault plane Σ_e of the small event is also taken to be a ramp function with a rise time τ_e and a final offset D_e. Now, the similarity condition in Eq. (4) shows that slip velocity may be assumed as a constant for most earthquakes of different sizes occurring in the same area. That is, we can write, *slip velocity* $=V_e=D/\tau=D_e/\tau_e$, or $D/D_e=\tau/\tau_e$ $=const\fallingdotseq N_D$.

When the above ratio is approximated by an integer, N_D, the following relation between the dislocation function of the large event and that of the small event is approximately made up as shown in **Fig. 3.**

$$\Delta U(\xi, \eta, t)=\sum_{k=1}^{N_D}\Delta U_e[\xi, \eta, t-(k-1)\tau_e], \tag{9}$$

and

$$\Delta\dot{U}(\xi, \eta, t)=\sum_{k=1}^{N_D}\Delta\dot{U}_e[\xi, \eta, t-(k-1)\tau_e].$$

Putting (9) into (8) and changing the order of the integral and the summation, we get,

$$S(\boldsymbol{x}, t)=\sum_{l=1}^{N_L}\sum_{m=1}^{N_W}\sum_{k=1}^{N_D}\mu\int_{\xi_l}^{\xi_l+L_e}\int_{\eta_m}^{\eta_m+W_e}\Delta\dot{U}_e[\xi, \eta, t-(k-1)\tau_e]. \tag{10}$$

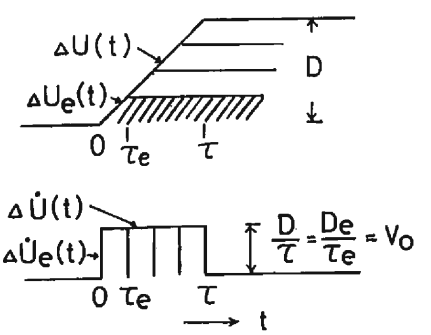

Fig. 3. The relations between the dislocation function of a large event and that of a small event and between their derivatives. $D/D_e=\tau/\tau_e\fallingdotseq N_D$ and N_D is approximated to be an integer.

The term expressed by the double integral is made of the source time function of the small event $S_{elm}(\boldsymbol{x}, t)$ having the starting point at a point (ξ_l, η_m). When the starting point of the large event is located at $(\mathbf{0}, \mathbf{0})$, we can write

$$S(\boldsymbol{x}, t)=\sum_{l=1}^{N_L}\sum_{m=1}^{N_W}\sum_{k=1}^{N_D} S_{elm}(\boldsymbol{x}, t-t_{dklm}), \tag{11}$$

where t_{dklm} is given as

$$t_{dklm}=r_{lm}/v_c+\sqrt{\xi_l^2+\eta_m^2}/v_r+(k-1)\tau_{elm}.$$

In the far-field, if each small event taking place on each element is assumed to have the same source mechanism, the source time function of each event may be regarded as approximately the same. Then we can rewrite (11),

$$S(\boldsymbol{x}, t)=\sum_{l=1}^{N_L}\sum_{m=1}^{N_W}\sum_{k=1}^{N_D} S_e(\boldsymbol{x}, t-t_{dklm}), \tag{12}$$

and

$$t_{dklm}=r_{lm}/v_c+\sqrt{\xi_l^2+\eta_m^2}/v_r+(k-1)\tau_e. \tag{13}$$

Equation (12) shows that the source time function $S(\boldsymbol{x}, t)$ for a large event may be approximated by the phase delayed summation of the source time function $S_e(\boldsymbol{x}, t)$ for asmall event.

Then the parameters N_L, N_W, N_D, v_r and τ_e can be estimated by employing the similarity conditions described in the above section. That is, N_L, N_W, N_D are determined from the cubic root of the moment ratio between the two earthquakes, $\sqrt[3]{M_0/M_{0e}}$. For the sake of the simplification for the computation, it is desirable for the cubic root value to be close to an integer.

2.3. Synthesis Method of Strong Ground Motions Using Observed Seismograms of Small Events

We will continue to use the Haskell model with a rectangular fault. The synthesis method of strong motions from a mainshock is developed as follows, using observed seismograms of small events such as foreshocks and aftershocks that occurred within the fault area of the mainshock. In order to simplify the expression, we assume that all small events used for the synthesis have the same moment. It is easy to modify the formulation obtained here for the case of using some events of different sizes.

Primarily, the ratio of the mainshock moment to the small-event moment, Mo/Mo_e, is determined. When the ratio Mo/Mo_e is N^3, the mainshock fault plane $\Sigma(=L\times W)$ is divided into $N\times N$ elements. Then, the area of an element, $\Delta\Sigma$, is taken as the fault size of the small event, $\Sigma_e(=L_e\times W_e)$. We call the element a subfault. The displacement U_e in the far-field caused by a subfault $\Delta\Sigma$ in an infinite homogeneous elastic medium is written in the form of

$$U_e(\boldsymbol{x}, t)=[R_c(\theta, \varphi)/4\pi\rho v_c^3 r]\cdot\mu\int_0^{L_e}\int_0^{W_e}\Delta U_e(\xi, \eta, t-t_c)d\xi d\eta, \tag{14}$$

where $t_c=r/v_c-\sqrt{\xi^2+\eta^2}/v_r$ and other notations are the same as in the previous section.

We consider the surface ground motions amplified by the effect of surface layering beneath an observation site. This transmission function due to the propagation medium is given by $T(\boldsymbol{x}, t)$. Then, if the contribution to the motions from the subfault is virtually equivalent to that from a point source, the surface motions $G_e(\boldsymbol{x}, t)$ are obtained by convolving $U_e(\boldsymbol{x}, t)$ with $T(\boldsymbol{x}, t)$. That is,

$$G_e(\boldsymbol{x}, t)=\int_{-\infty}^{\infty} T(\boldsymbol{x}, t-t')\cdot U_e(\boldsymbol{x}, t')dt' \tag{15}$$

Accordingly, the ground motions G_{elm} which result from the dislocation ΔU_{elm} of a small event on an arbitrary element $\Delta\Sigma_{lm}$ located at (ξ_l, η_m), as shown in **Fig. 4,** are written by

$$G_{elm}(\boldsymbol{x}, t)=T_{lm}(\boldsymbol{x}, t)*c_{lm}\mu\int_{\xi_l}^{\xi_l+L_e}\int_{\eta_m}^{\eta_m+W_e}\Delta\dot{U}_{elm}(\xi, \eta, t-t_{clm})d\xi d\eta, \tag{16}$$

where $t_{clm}=r_{lm}/v_c+\sqrt{(\xi-\xi_l)^2+(\eta-\eta_m)^2}/v_r$, and
$c_{lm}=(1/4\pi\rho v_c^3)R_{clm}(\theta_{lm}, \varphi_{lm})/r_{lm}$.

On the other hand, the contribution to the mainshock motions, G_{lm}, due to the dislocation ΔU_{lm} on an element $\Delta\Sigma_{lm}$ during the mainshock are written by

$$G_{lm}(\boldsymbol{x}, t)=T_{lm}(\boldsymbol{x}, t)*c_{lm}\mu\int_{\xi_l}^{\xi_l+L_e}\int_{\eta_m}^{\eta_m+W_e}\Delta\dot{U}_{lm}(\xi, \eta, t-t_{clm}). \tag{17}$$

The relation between the dislocation function of the mainshock, $\Delta\dot{U}_{lm}$, and that of the small event, $\Delta\dot{U}_{elm}$, has been given by (9) from the similarity condition. We get from (9), (16) and (17),

$$G_{lm}(\boldsymbol{x}, t)=\sum_{k=1}^{N_D} G_{elm}[\boldsymbol{x}, t-(k-1)\tau_{elm}]. \tag{18}$$

Thus, the surface motions $G(x, t)$ from the mainshock are given by the time-lagged summation of G_{lm} over the fault plane, that is,

$$G(\boldsymbol{x}, t)=\sum_{l=1}^{N_L}\sum_{m=1}^{N_W} G_{lm}(\boldsymbol{x}, t-t_{clm})=\sum_{l=1}^{N_L}\sum_{m=1}^{N_W}\sum_{k=1}^{N_D} G_{elm}(\boldsymbol{x}, t-t_{dklm}) \tag{19}$$

where t_{dklm} is given as

$$t_{dklm}=r_{lm}/v_c+\sqrt{\xi_l^2+\eta_m^2}/v_r+(k-1)\tau_{elm}. \tag{20}$$

Then, the ground motions $G(\boldsymbol{x}, t)$ from the mainshock can be calculated from (19), if all the records at a given site from every event corresponding to every element were obtained.

Now, a synthesis method is developed using seismograms from a few small events which occurred within the fault area of the mainshock. We consider a case of obtaining only one seismogram from a small event corresponding to a subfault

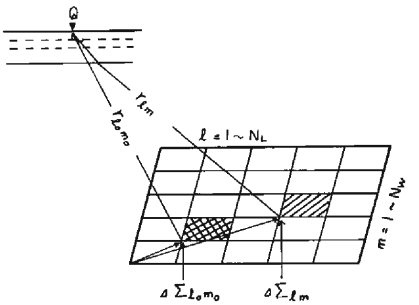

Fig. 4. Geometrical relation between the fault element $\Delta\Sigma_{lomo}$ of an observed small event and the observed point Q.

$\Delta\Sigma_{lomo}$ as shown in **Fig. 4.** The ground motions G_{elm} from an arbitrary element may be estimated from the observed motions G_{elomo} in the following equation, if the propagation effect T_{lm} is approximately equal to T_{lomo}:

$$G_{elm}(\boldsymbol{x}, t) = [R_c(\theta_{lm}, \varphi_{lm})/R_c(\theta_{lomo}, \varphi_{lomo})](r_{lomo}/r_{lm})G_{elomo}(\boldsymbol{x}, t-t_{elm}),$$
$$t_{elm} = (r_{lm}-r_{lomo})/v_c \tag{21}$$

Putting (21) into (20), the surface motions $G(\boldsymbol{x}, t)$ from the mainshock are given by

$$G(\boldsymbol{x}, t) = \sum_{l=1}^{N}\sum_{m=1}^{N}\sum_{k=1}^{N}[R_c(\theta_{lm}, \varphi_{lm})/R_{ce}(\theta_{lomo}, \varphi_{lomo})]\cdot(r_{lomo}/r_{lm}) \cdot G_{elomo}(\boldsymbol{x}, t-t_{elm}-t_{dklm}). \tag{22}$$

We can easily improve this synthesis method for the case of using seismograms from several events. When the synthesis is made from the several events with different moments, some care must be taken of scaling the observed data for the moment in regard to the element size and the number of summation.

The starting point in this formulation is taken to be the origin of the coordinate (ξ, η) on the mainshock fault. When the starting point is located at an arbitrary point (ξ_o, η_o), it is necessary to change the t_{dklm} as follows:

$$t_{dklm} = r_{lm}/v_c + \sqrt{(\xi_l-\xi_o)^2+(\eta_m-\eta_o)^2}/v_r + (k-1)\tau_{elm} \tag{23}$$

Now we consider the extent of the validity of this synthesis formulation. The ground motions from an arbitrary element shown by (16) and (17) can be usually represented when the observed wavelength is much longer than the source-space dimension-i.e. when the point source approximation is valid. In the case of considering the ground motions by separating P and S wave parts, even if the source size is greater than a wavelength, as long as the distance between the source and the receiver is much greater than the source dimension, the effect of the finite source size can also be separated as discussed in chapter 14 of Aki and Richard (1980)[30]. That is, the approximation by (16) and (17) is justified for

$$L_e^2 \ll \lambda r/2, \tag{24}$$

where L_e is the length of the element source, i.e. the fault length of the small event, λ, the wave length and r, the distance between source and receiver. This relation determines the extent of the validity of the distance and the wavelength in the synthesis formulation obtained here. If the records from the smaller events with the smaller fault lengths are used, this synthesis method is effective up to the shorter wavelength and up to the shorter distance from the fault. It must be cautioned that if the motions of various wave types coexist, this will lower the accuracy of the approximation of this formulation. We consider this synthesis is valid for the S wave motions which constitute the main parts of the strong ground motions. The extension to the case of surface waves is easily made after slight modification.

2.4. Numerical Check of Synthesis Method

The source time functions of earthquakes are calculated here as a superposition of contribution from $\Delta\dot{U}$ at infinitesimal surface elements $d\Sigma$, i.e. (7).

Our formulation for the synthesis of strong ground motions is based on an idea that the source time function of a large event can be expressed by a superposition of the source time functions of small events having certain fault dimensions, without direct estimation of $\Delta\dot{U}$ for the large event, i.e. (12). We need to examine the frequency range, of seismic waves radiated from the fault, in which equation (12) can be valid as an approximation, relating to the number of small events used and the element sizes corresponding to the fault dimensions of small events. For this purpose, the source time function given by direct numerical-integral of $\Delta\dot{U}$ on the mainshock fault plane, i.e. (7), is compared with the source time function synthesized by (12) and (13) using that of small events. The source time function of each small events is calculated by the integral of (7), given $\Delta\dot{U}_e$ for the small event. We call the former, theoretical seismogram and the latter, synthesized seismogram for convenience.

Now, we will examine the range of applicability of our formulation for the following 3 cases shown in **Fig. 5.**

1. Model H1–1: rupture starts at $x=0$ simultaneously over the whole width W of

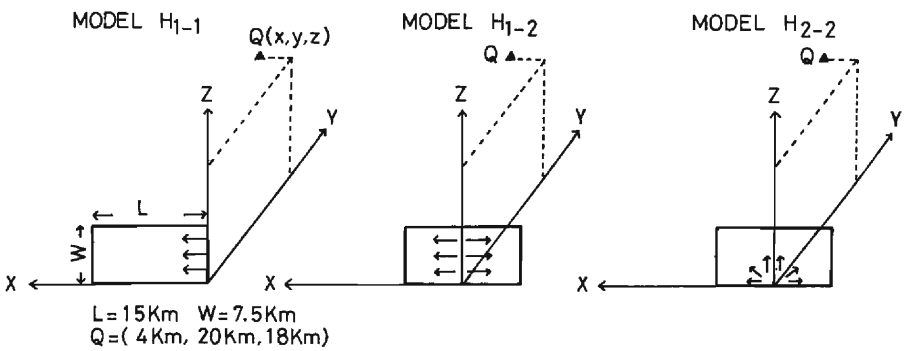

Fig. 5. Three fault models used for numerical check of synthesis method.

the fault and extends unilaterally at a constant rupture velocity.

2. Model H1–2: rupture extends bilaterally. The others are the same as H1–1.
3. Model H2–2: rupture extends circularly from a point.

The rectangular fault, $L=2W$ (L: length and W: width), and $\Delta U(x, y, t)$ with a linear ramp function uniformly over the fault plane are assumed as being the same in all three cases. The fault dimension, the rise time and the relative location of the fault plane and the observational point are taken to coincide with the case of the observed seismograms at the JIZ station during the 1980 Izu-Hanto-Toho-Oki earthquake, which will be analyzed in the next section. That is, $L=15$ km, $W=7.5$ km, $\tau=1$ sec, the coordinate of the observed point $=(4$ km, 20 km, 18 km)

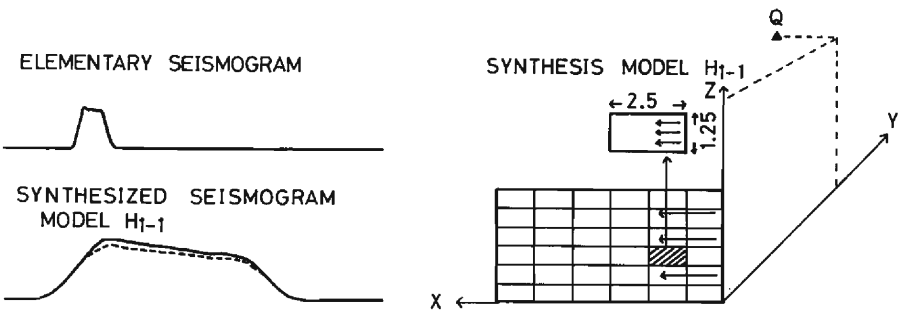

Fig. 6. Comparison between 'theoretical' seismogram and 'synthesized' one for model H1-1 drawn in the right figure. The 'theoretical' seismogram is calculated as a superposition of contribution from ΔU at an infinitesimal element $d\Sigma$ over the whole fault plane and an elementary seismogram is calculated in the same manner over the hatched plane. The 'synthesized' seismogram is calculated by the delay and summation of the elementary seismogram, following (11).

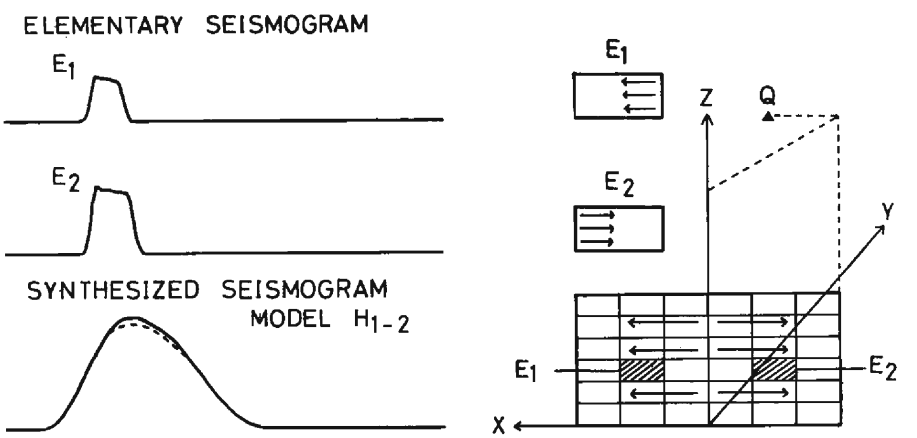

Fig. 7. Comparison between 'theoretical' seismogram and 'synthesized' one for model H1-2 drawn in the right figure. Two events, E1 and E2 are used as elementary earthquakes for synthesis. The calculated method is similar to the method described in Fig. 6.

when the starting point is the origin. The moment ratio between the mainshock and the small events is 6^3. Since the similarity condition (4) is assumed to be valid, the mainshock fault plane is divided into 6×6 elements and the element size of the small event is taken as $L_e=2.5$ km and $W_e=1.25$ km, and the rise time, $\tau_e=\tau/6=0.166$ sec.

The theoretical seismogram and the synthesized seismogram are compared in **Figs. 6, 7 and 8.** In each figure, the left upper (one seismogram in **Fig. 6** and two seismograms in **Figs. 7 and 8**) shows the small event seismograms generated from subfaults depicted by hatched areas, and the left bottom shows the mainshock seismogram synthesized using the small event ones. The number of the small events for this synthesis is one for H1–1 and two for H1–2 and H2–2. The theoretical seismogram for each model is drawn by a dotted curve together with the synthesized one. In all figures, the seismograms calculated by two different methods almost agree and the discrepancy of the maximum amplitude between the two waveforms is within 10%. The Fourier spectra of the theoretical and synthesized ones are compared in **Fig. 9.** The spectra calculated by the two methods are in good agreement in the frequency range lower than 1 Hz and rough agreement in the frequency range higher than 1 Hz, although the two spectra have some discrepancies in detail. The higher limit of the frequency in which this synthesis method is applicable may be near 6 Hz, i.e. $1/\tau_e$.

These results show that the synthesis method given by (12) is applicable for estimating the source time function of the mainshock in the wide frequency range even at the short distance comparable to the fault length if the Haskell-type model is valid for actual earthquakes. We consider the Model H2–2 to be more realistic for actual earthquakes than the Models H1–1 and H1–2, because difficulties in

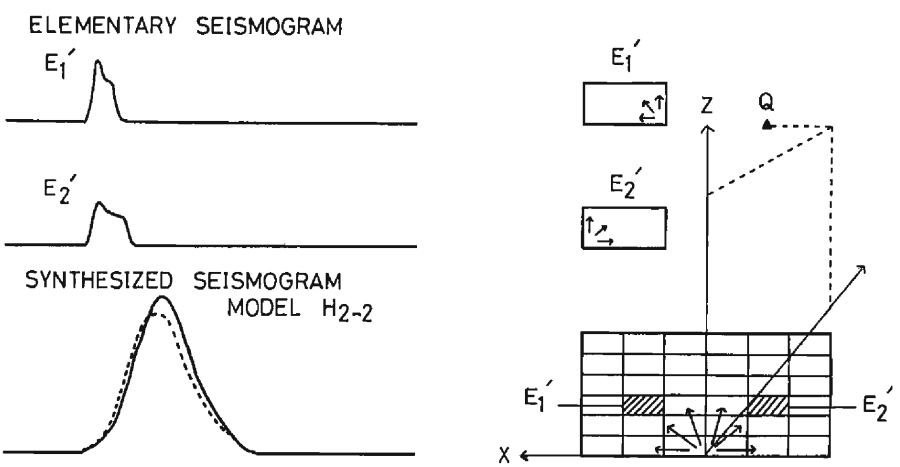

Fig. 8. Comparison between 'theoretical' seismogram and 'synthesized' one for model H2-2 drawn in the right figure. Two events E1′ and E2′ are used as elementary earthquakes for synthesis. The calculated method is similar to the method discribed in Fig. 6.

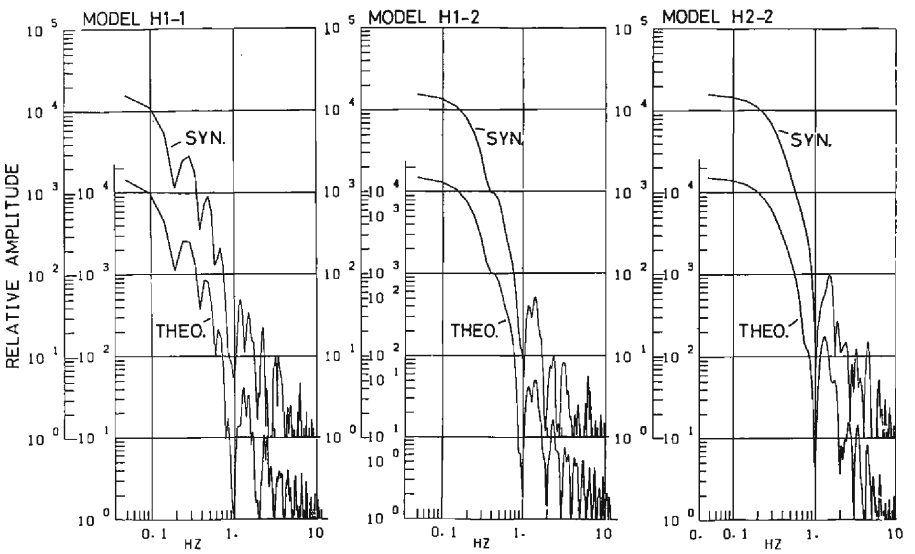

Fig. 9. Comparison between Fourier spectra of 'theoretical' seismograms and those of 'synthesized' sesmograms for the three models shown in Fig. 5. 'SYN.' and 'THEO.' in figures indicate 'theoretical' and 'synthesized', respectively.

unlimited rupture velocity toward the z-direction can be avoided in this model. However, the accuracy of the approximation of the synthesis in the Model H2–2 shown in **Fig. 8** drops to some extent compared with that of H1–1 and H1–2, shown in **Fig. 6 and 7.** We have to take care in the case of the synthesis for higher frequency motions. If a larger number of smaller events appropriately distributed over the fault are used for the synthesis, the approximation is improvable. However, another problem is indicated by Chouet et al. (1978)[31] that the similarity assumptions of earthquakes show some departures for smaller earthquakes. Thus, for our synthesis we should use small earthquakes with appropriate size which can be related to the mainshock in accordance with the similarity condition.

We have not been checking here the synthesis formulation (19) or (22). This examination needs the calculation of the theoretical seismograms, taking into account on the propagation effects due to the geological structure of the medium, for example, those given by Refs. (5)—(7) and (9). This calculation is too complicated and immense, while our synthesis method needs only a simple and small quantity of computation. In case of regarding the propagation effects of seismic waves from each element to the station as being approximately invariant to one another, the synthesis formulation (19) become equivalent to (12), when S_e is considered to be a small event seismogram. From the simple numerical check mentioned above, we can estimate a rough extent of the applicability for our synthesis method.

3. Synthesis of the Velocity Motions from the Mainshock (M=6.7) of the 1980 Izu-Hanto-Toho-Oki earthquake

3.1. Observed Data

A shallow earthquake with a magnitude of 6.7 (the 1980 Izu-Hanto-Toho-Oki earthquake) occurred on June 29, 1980, off the east coast of the Izu Peninsula. We obtained the velocity seismograms from the mainshock as well as small events such as foreshocks and aftershocks at three sites located at short distances from about 20 km to 100 km, which were recorded by velocity-type strong-motion-seismographs designed by Muramatu (Muramatu, 1977)[32]. The maximum velocity of 8 kine was recorded at the JIZ station on hard rock, about 20 km away from the epicenter.[33] The locations of the observed stations, JIZ, SMC and OMM are shown by (+) mark in **Fig. 10.** The observation system was designed to record exactly ground velocity motions with the dynamic range from 100 to 0.01 kines over the period range from 0.05 to 50 second. These seismograms obtained by the velocity-type strong-motion-seismograph are useful for predicting the ground motions from large earthquakes, since they have a wide dynamic range over a wide period range.

An active earthquake swarm occurred in a small area north of the mainshock

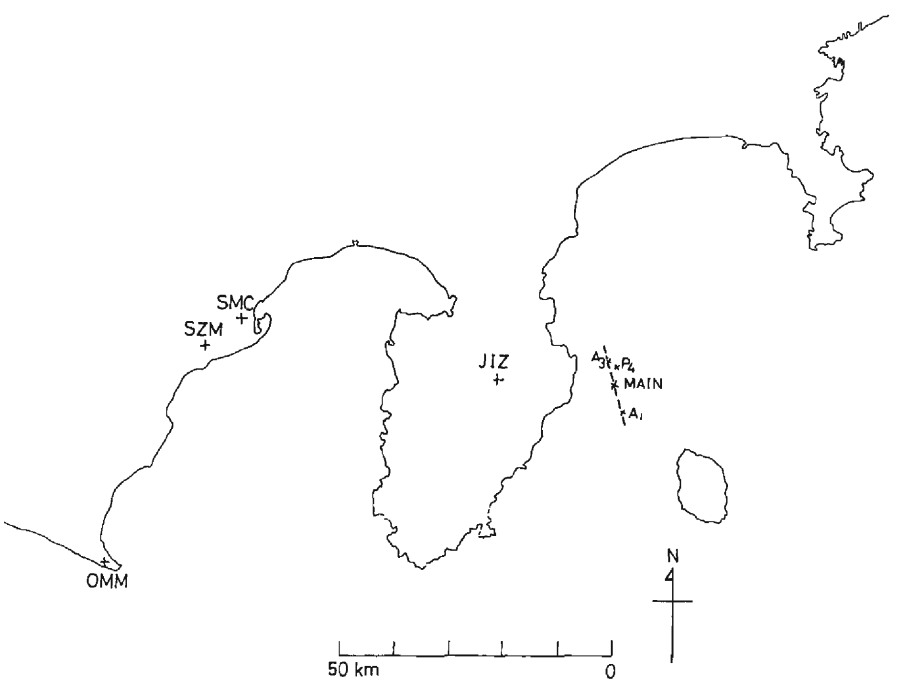

Fig. 10. The location of the observation sites and the epicenters of the mainshock and the small events used for synthesis. The mainshock is the 1980 Izu-Hanto-Toho-Oki earthquake with M=6.7.

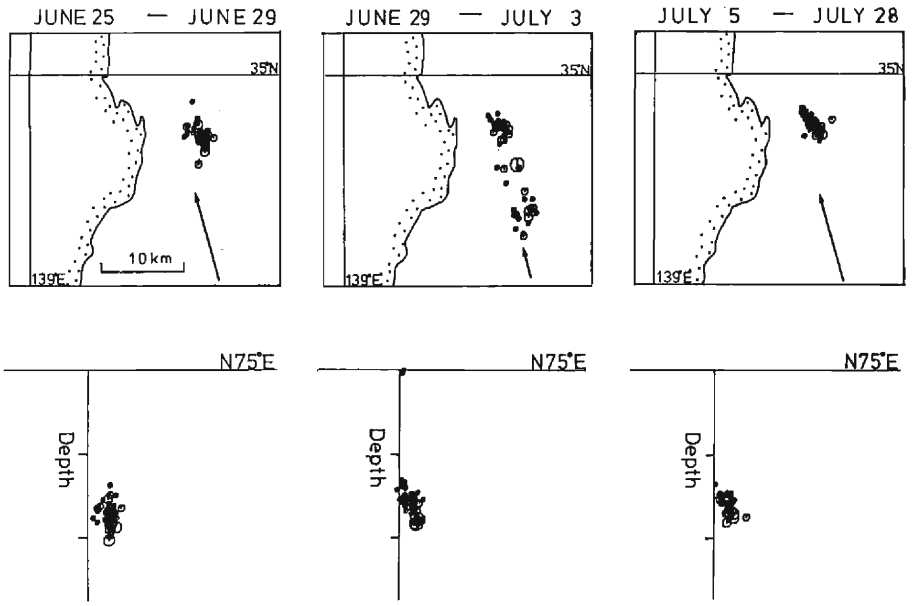

Fig. 11. Hypocentral distribution of earthquakes for the three period, 1) before the mainshock, 2) within 5 days after the mainshock, 3) after that. (after Imoto et al. 1981[32])

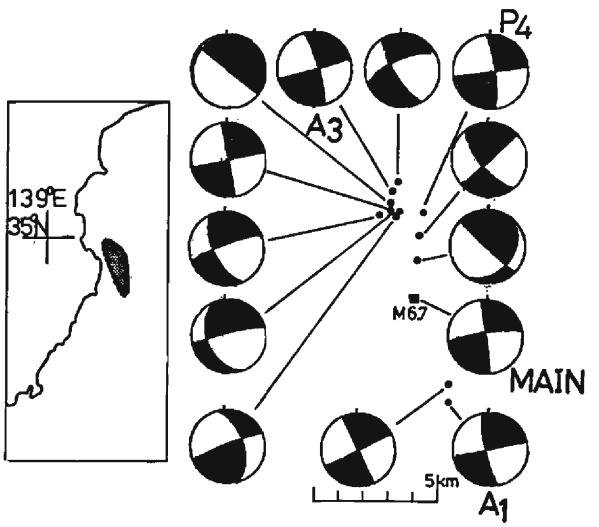

Fig. 12. Fault plane solutions of large earthquake ($M>4.0$) projected on the lower hemisphere of equal arc projection. Dark and light areas indicate compressional and dilatational quadrants, respectively. (after Imoto et al. 1981[32])

hypocenter for about 40 days before and after the mainshock. The focal mechanisms of the earthquake swarm were studied by Imoto et al. (1980)[34]. They plotted the hypocentral distribution of the earthquakes, as shown in **Fig. 11,** classifying the events into three periods, (1), before the largest shock of the mainshock, (2), within 5 days after the largest shock, and (3), after that. The aftershocks immediately after the largest shock, or in the second period, are distributed within the range of about 15 km in length along the direction N15°W and 12–19 km in depth.

We presumed the fault plane, $L=15$ km and $W=7.5$ km, from the hypocentral distribution of aftershocks in the second period. In **Fig. 10,** the inferred fault is indicated by a dotted line, and the epicenters of the mainshock, the foreshocks and aftershocks employed for the present synthesis are shown by ($\times$) marks. The fault plane solutions of the earthquakes with the magnitude larger than 4 determined by Imoto et al. are shown in **Fig. 12,** projected on the lower hemisphere of the equal arc projection. Most of the earthquakes as well as the mainshock show strike-slip type mechanisms.

3.2. Estimates of the Fault Parameters for the Synthesis

The synthesis of the mainshock motions is made, using (22), from the observed seismograms of foreshocks and aftershocks. It is necessary to determine the following parameters for the synthesis.

(a) The fault dimension of the mainshock synthesized, (the length L and the width W) and the fault geometry.
(b) The moment ratios, Mo/Mo_s, between the mainshock and the small events.
(c) The rise time, τ(or τ_e), of either the mainshock or the small events.
(d) The rupture velocity, v_r.

The parameters in this study were determined from the hypocentral distribution of aftershocks, the Fourier Spectra of observed seismograms and the similarity conditions of fault parameters. For the purpose of predicting strong ground motions for a future large earthquake, these parameters have to be supplied from maps of geology and seismicity and the similarity conditions for a given seismic region.

We summarize the fault dimension and the geometry in **Table 1**, according to descriptions in the foregoing section.

The fault dimension and geometry of (a) are estimated from the aftershocks' distribution as described in the above section.

The moment ratios of (b) are estimated from the spectral ratios between the mainshock and small events. The observed seismograms and the Fourier spectra

Table 1 The fault parameters of the 1980 Izu-Hanto-Toho-Oki earthquake

strike	N15°W	fault length	15 km
dip	90°	fault width	7.5 km
		rise time	1.0 sec
		rupture velocity	3.2 km/sec

of the mainshock and the aftershocks (A1 and A3) at JIZ are shown in **Fig. 13** and **Fig. 14.** The spectral ratios between the mainshock and the two aftershocks are shown in **Fig. 15.** The observed seismograms, the Fourier spectra of the mainshock, foreshock P4 and aftershock A1 at SMC are shown in **Fig. 16** and **Fig. 17** and the spectral ratios are shown in **Fig. 18.** The seismic moment is estimated from the low frequency level of the spectra, based on the dislocation theory. Accordingly, the moment ratio Mo/Mo_e is given from the flat level, in the low frequency range, of the spectral ratio shown in **Fig. 15** and **Fig. 18.** The spectral ratio of the mainshock to aftershock A1 is estimated to be about 200 ($\approx 6^3$) at the JIZ site and at the SMC site as well. Similarly, the moment ratio of the mainshock to aftershock A3 is given to be about 350 ($\approx 7^3$) and that of the mainshock to foreshock P4, about 200 ($\approx 6^3$).

Then, the scaling parameter N ($\approx \sqrt[3]{Mo/Mo_e}$) corresponding to the ratio of fault lengths between the two earthquakes (see eq. (4)) is estimated to be 6 for the mainshock versus A1, 7 for the mainshock versus A3 and 6 for the mainshock versus P4.

The rise time of (c) is estimated as follows. The spectra of the Haskell-type fault model, based on the dislocation with a ramp function are characterized by a signifi-

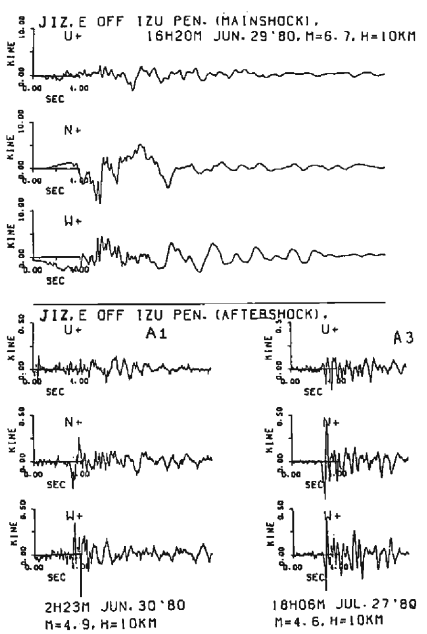

Fig. 13. The observed seismograms of the mainshock and two aftershocks A1 and A3, at the JIZ station.

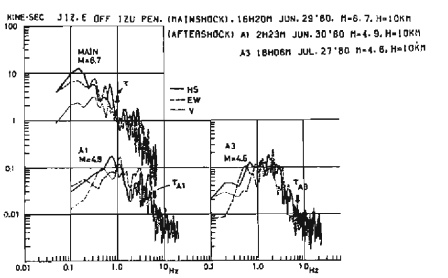

Fig. 14. The Fourier spectra of the mainshock and two aftershocks, A1 and A3, at the JIZ station.

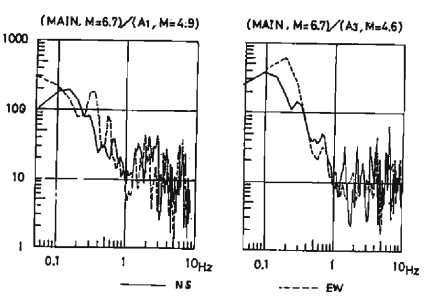

Fig. 15. The spectral ratios between the mainshock and aftershock A1 and between the mainshock and aftershock A3 at the JIZ station.

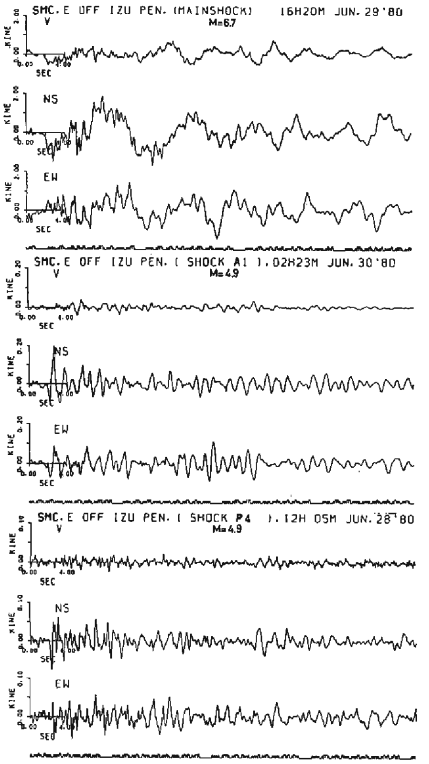

Fig. 16. The observed seismograms of the mainshock, aftershock A1 and foreshock P4 at the SMC station.

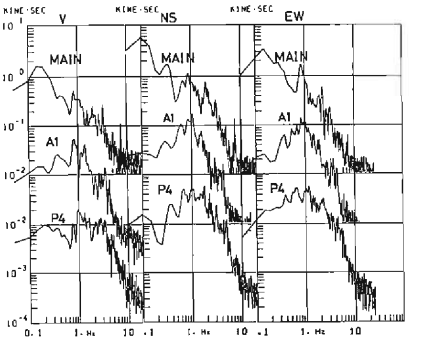

Fig. 17. The Fourier spectra of the mainshock and aftershock A1 and foreshock P4 at the SMC station.

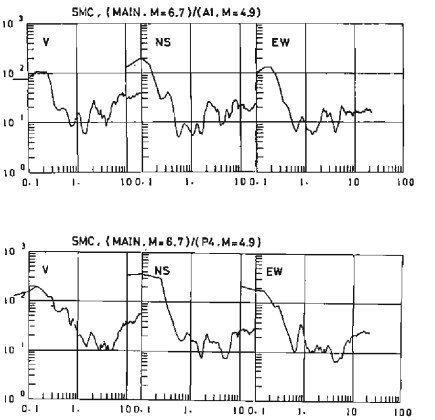

Fig. 18. The spectral ratios between the mainshock and aftershock A1 and between the mainshock and foreshock P4 at the SMC station.

cant trough around $1/\tau$ (τ: rise time) as well as by the corner frequency related to the fault dimension, as clearly shown in **Fig. 9.** However, the rise time determined by picking the trough frequency has larger uncertainties and may often be non-unique, because the spectra of far-field observation data are strongly modified by scattering and absorption in the propagation medium and further by local ground effects. Therefore, some care has been taken to estimate the rise time.

The JIZ station is in a drift formed of a hard rock and at a short-distance of about 20 km away from the epicenter. We consider the seismograms obtained at JIZ to be less influenced by the propagation effect. In **Fig. 14,** the spectra of the mainshock at JIZ have a common significant trough around 1 Hz for the NS, EW and V components. On the other hand, the spectra of aftershocks A1 and A3 have no significant trough around 1 Hz. Thus, the trough around 1 Hz for the mainshock

may be independent of the local ground effects. The troughs of the spectra for aftershocks A1 and A3 appear to be at about 6 Hz and 7 Hz as indicated by arrows although they are not so significant, as compared with the case of the mainshock. After the above considerations, we determine the rise time of the mainshock to be 1 sec. Since the trough frequencies of the aftershock are non-unique, we determine the rise times to be consistent with the similarity condition, i.e. 1/6 sec for A1 and 1/7 sec for A3. These values also correspond to the trough frequencies shown by arrow marks in **Fig. 14.**

In the section 2.1, we noted that the rise time is given from the similarity relation (5). The rise time is obtained to be about 1.2 sec when the inferred fault plane area of the mainshock and S wave velocity of the medium are put into (5). This value is very close to the rise time estimated here from the spectral shapes of the observed seismograms in the short distance. Thus, in the synthesis we may use the value of the time given by the relation (5) as a first approximation.

We do not have any evidence for v_r estimates, but tentatively assume to be 3.0 km/sec, based on the empirical data. The validity of this assumption is later examined by a comparison between the synthesized seismograms and the observed spectra.

3.3. Synthesis Results

The hypocenter of the mainshock is located at the center bottom of the fault plane inferred from the aftershocks' distribution shown in **Fig. 11.** We consider that this hypocenter is consistent with the starting point of a rupture and that the rupture spreads circularly from the starting point, P_o, over the fault plane. That is, this type of rupture propagation corresponds to that for Model H2–2 shown in **Fig. 5.** The locations of the hypocenters of the mainshock and the small events employed for the synthesis are summarized in **Table 2.**

First, we describe the synthesis of the mainshock motions at SMC. We use the seismograms from two small earthquakes; one is event P4 with $M=4.9$ in an area north of P_o and the other is event A1 with the same magnitude in an area south of P_o. The locations of the epicenters of A1 and P4, and the mainshock fault plane are shown in **Fig. 10.** The fault plane solutions of A1 and P4 are similar to those of the mainshock as shown in **Fig. 12.** The moment ratios of the mainshock of $M=6.7$ to events P4 and A1 are estimated from the spectral ratios to be $Mo/Mo_e=N^3\approx200$,

Table 2 The origin times and hypocenter of the earthquakes used for the synthesis. (after Imoto et al., 1981[34])

	M	D	H	M	LAT. (deg.)	LONG. (deg.)	DEPTH (km)	MAG. (JMA)
P4	6	28	12	5	34.934	139.234	18.9	4.9
MAIN	6	29	16	20	34.904	139.230	17.9	6.7
A1	6	30	2	23	34.847	139.245	18.4	4.9
A3	7	27	18	6	34.942	139.220	17.3	4.6

which yields the scaling parameter $N \approx 6$. Then the fault plane of the mainshock is divided into 6×6 elements as shown in **Fig. 19.** The rise time of the mainshock is estimated to be 1 sec as mentioned in section 3.2. The rise time of each small event, τ_e, is estimated to be τ/N, from the similarity condition. The correction factors for the radiation amplitudes $R_c(\theta_{lm}, \varphi_{lm})/R_{ce}(\theta_{lom_o}, \varphi_{lom_o})$ are taken to be unity as a first approximation for simplification of the computation.

We make deterministically a synthesis for the mainshock motions in the following two stages. In the first stage, the

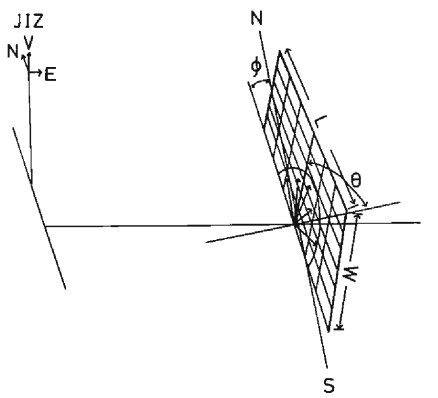

Fig. 19. The schematic model of the fault plane for synthesis. Rupture spreads cocircularly from Po.

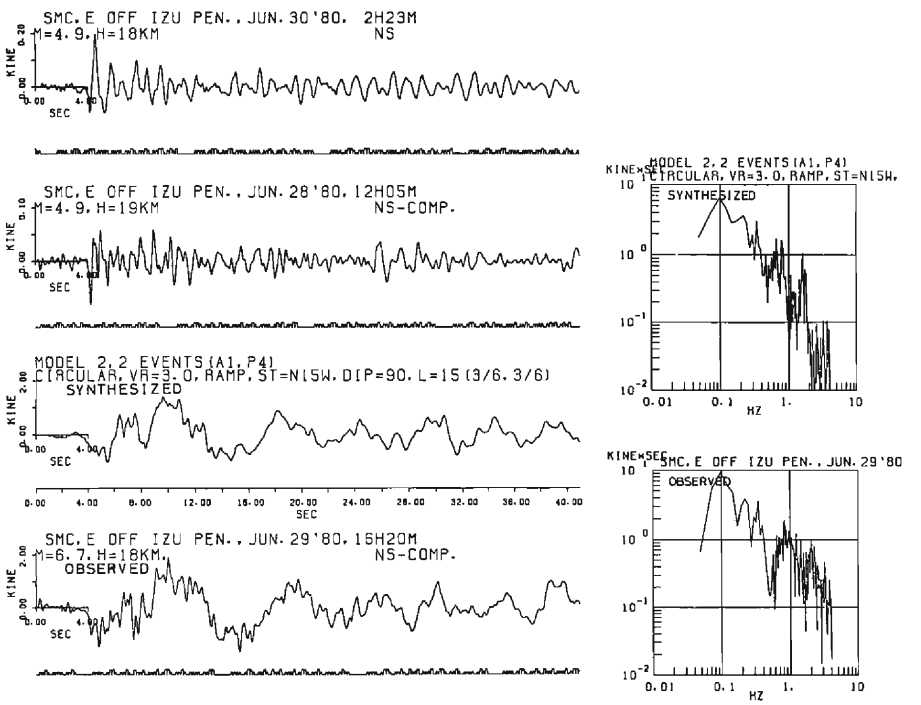

Fig. 20. Comparison of the synthesized velocity seismogram with the observed one for the mainshock at the SMC station. The left upper two traces are the observed seismograms of aftershock A1 and foreshock P4 used as elementary earthquakes, the left third trace, the synthesized seismogram for the mainshock, and the left bottom trace, the observed seismogram of the mainshock. The right upper figure is the Fourier spectrum of the synthesized seismogram and the right lower figure is that of the observed mainshock seismogram.

mainshock fault plane is divided into two areas, one is S_1 for the northern half area, the other, S_2 for the southern half area, each of which has 3×6 elements, respectively. The synthesized seismogram f_1 is obtained, using P4 for S_1 and f_2, using A1 for S_2, respectively. In the second stage, after summing up f_1 and f_2, we obtain the synthesized mainshock motions.

The synthesized velocity seismogram of the NS component for the SMC station is shown in **Fig. 20,** together with the observed seismogram of the mainshock. The upper two are the P4 and A1 seismograms used as elementary earthquakes, the third is the synthesized and the fourth is the observed seismograms. These are outputs from a 4 Hz low-pass-filter, by which an apparent predominant frequency of $1/\tau_e$ ($=6$ Hz) involved in the synthesized seismogram has been removed. This periodic motion is discussed in later section. It is found that the synthesized seismogram is in good agreement with the observed seismogram, except for a few portions with periods around 1 sec.

Similarly, the synthesis of the mainshock velocity motions is made for OMM using P4 and A1 and for JIZ using A3 and A1 (because event P4 failed to be observed

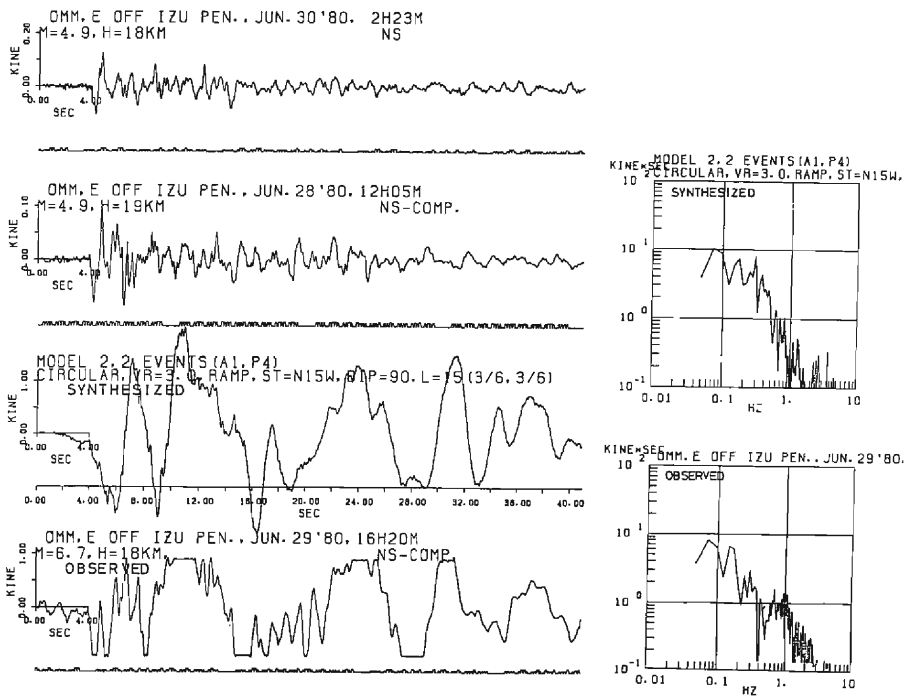

Fig. 21. Comparison of the synthesized velocity seismogram with the observed one for the mainshock at the OMM station. The arrangement of the figures is the same as that of Fig. 20. The observed seismogram at the OMM station from the mainshock is recorded in a saturated form over 1 kine because of poor conditions of the auto-gain-control system.

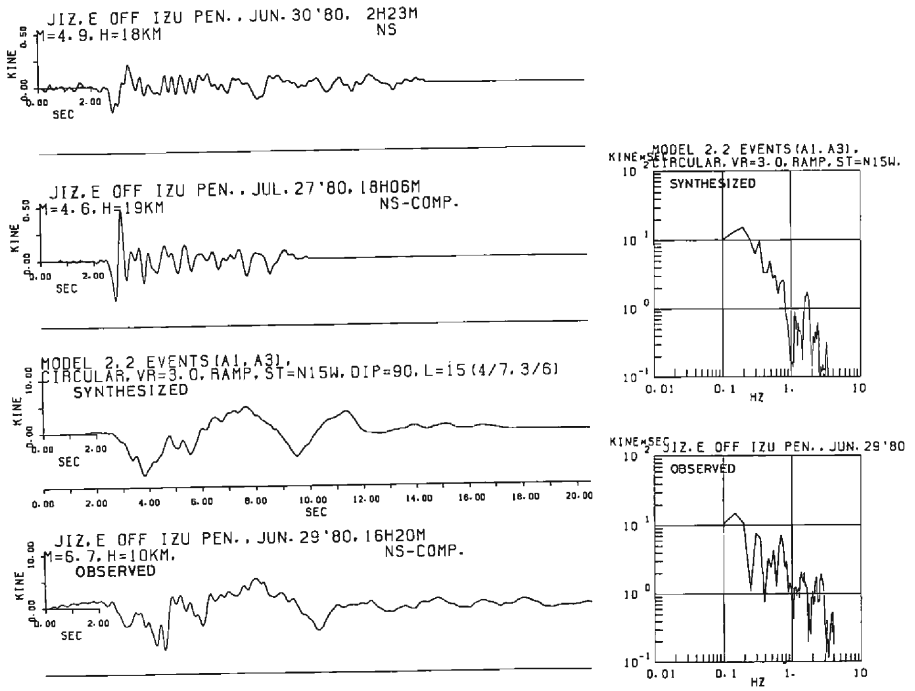

Fig. 22. Comparison of the synthesized velocity seismogram with the observed one for the mainshock at the JIZ station. The arrangement of the figures is the same as that of Fig. 20.

at the JIZ station). These results are shown in **Fig. 21** and **22.** The moment ratio of the mainshock to A3 is almost 350 and then the scaling factor is estimated to be 7. For this reason, the northern half area S_1 is divided into 4×7 ($\fallingdotseq N/2\times N$ for $N=7$). The synthesized seismogram at OMM is also in good agreement with the observed one, similar to the case of SMC. The synthesized seismogram at JIZ agrees well with the observed one, inclusive of portions with periods around 1 sec, although the spectral amplitudes of the synthesized one higher than 1 Hz are underestimated as compared with those of the observed one.

To examine the validity of the assumed parameters, we calculate the synthesized seismograms for a function of each parameter, and compare them with the observed one in the time domain. Three kinds of measure to evaluate coincidence between the synthesized seismogram $f(t)$ and the observed one $g(t)$ are used: correlation function ϕ, amplitude ratio a, and residual function r, where these parameters are defined as,

$$\phi=\left[\int_0^T f(t')\,g(t-t')dt' \Big/ \left(\int_0^T f^2(t)dt\int_0^T g^2(t)dt\right)^{1/2}\right]$$

$$a=\left[\int_0^T f^2dt \Big/ \int_0^T g^2dt\right]^{1/2}$$

$$r=\int_0^T (f-g)^2dt \Big/ \left(\int_0^T f^2dt\int_0^T g^2dt\right)^{1/2}$$

We determine an optimum model by changing three parameters in the following order: (1) the relative position of the starting point on the mainshock fault plane, (2) the rupture velocity and (3) the rise time. The fault geometry, and the number of the elements assigned are fixed in all cases.

Examinations with regard to the location of the starting point P_0 are shown in **Fig. 23** for the cases of the SMC and JIZ station. Let the coordinate of P_0 be (x, y), located at a grid point on the fault plane as shown in the right upper figure. ϕ, a and r are computed for the time length of 40 sec for SMC and 12 sec for JIZ after low-pass-filtering with a cut-off-frequency of 4 Hz. **Fig. 23** shows that, when P_0 is located at (3, 0), the correlation is clearly highest, the amplitude ratio is closest to unity and the residual is least, although those values are different for SMC and JIZ. The difference of ϕ, a and r for the two stations is mainly due to the difference in the data length used. This optimum location of the starting point is consistent with the relative position of the mainshock hypocenter within the distribution area of aftershocks in **Fig. 11.**

Similar examinations with regard to the rupture velocity V_r are shown in **Fig. 24**, when the starting point is located at (3, 0). The influence on the waveform due

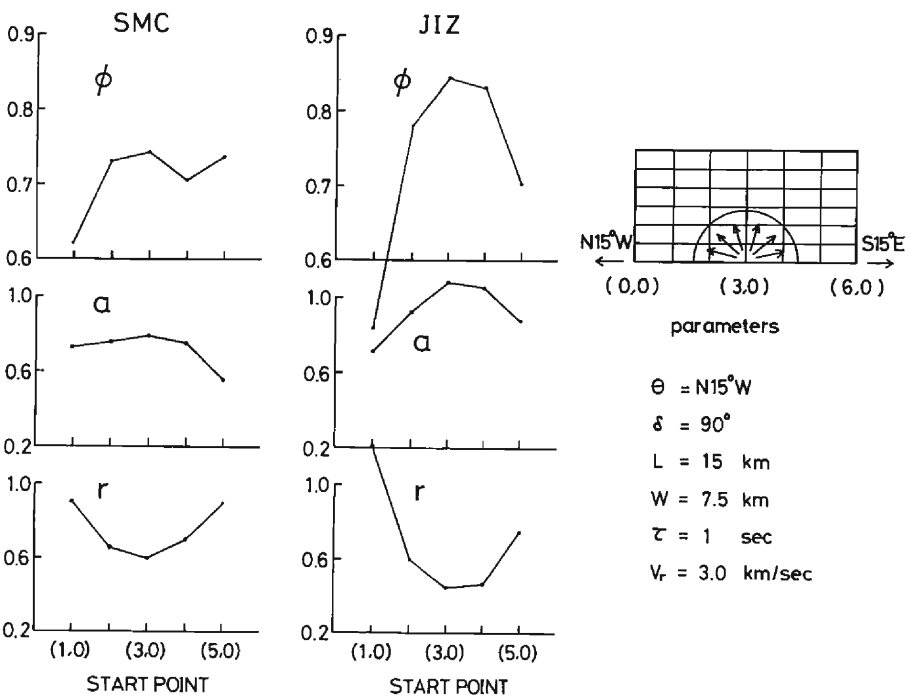

Fig. 23. The examination of the variation of the synthesized seismograms due to the location of the starting point within the fault plane. ϕ, a and r are correlation function, amplitude ratio and residual function between the synthesized seismogram for the starting point varying from (0, 0) to(6, 0) at the fault plane, as shown in the right upper figure, and the observed seismogram.

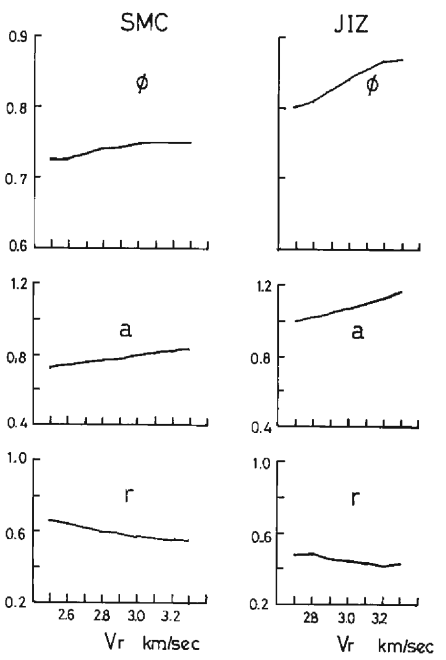

Fig. 24. The examination of the variation of the synthesized seismograms due to the rupture velocity.

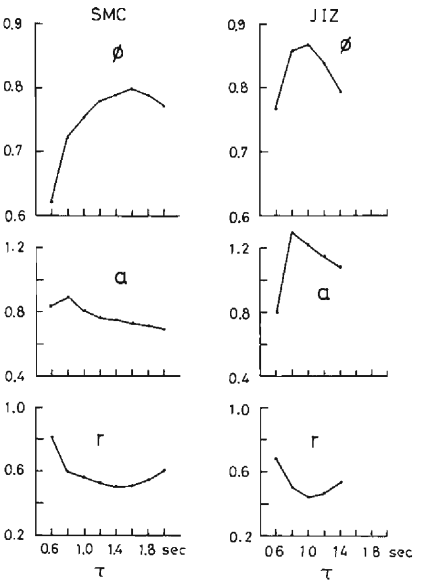

Fig. 25. The examination of the variation of the synthesized seismograms due to the rise time of the mainshock. In the synthesis, the relation, $\tau_e=\tau/N$, is kept between the rise time of elementary earthquakes and that of the mainshock,.

to the change in the rupture velocity, ranging between 2.8 and 3.3 km/sec is found to be very little. We may not have the resolution enough to determine the rupture velocity from this analysis. We have chosen $V_r=3.2$ km/sec as the optimum which gives the minimum residual value.

In order to examine the validity of the rise-time value of the mainshock, the influence on the synthesized waveform due to the change in the rise time ranging 0.6 to 2.0 km/sec is shown in **Fig. 25.** The rise time of elementary earthquakes is estimated from the similarty condition $\tau_e=\tau/N$. For the case of the JIZ station, the optimum value from the correlation and the residual function is given to be 1.0 sec, which is consistent with the estimated value from the spectral shape at JIZ, as mentioned in section 3.1. On the other hand, the rise time for the case of SMC is given to have best fit for about 1.5 sec, which is somewhat larger than that for JIZ. For the case of SMC, the synthesized seismogram having $\tau=1.5$ sec is compared with the observed one in **Fig. 26.** It seems that the waveform and spectra of the sybthesized with $\tau=1.5$ sec are in better agreement with those of the observed, inclusive of the period range from 1 to 1.5 sec, while its range is in disagreement between the synthesized and the observed in **Fig. 20.** For the case of OMM we obtain better fit for $\tau=1.5$ sec rather than $\tau=1.0$ from the comparison between the synthesized and the observed (we can not accurately compute the correlation and residual

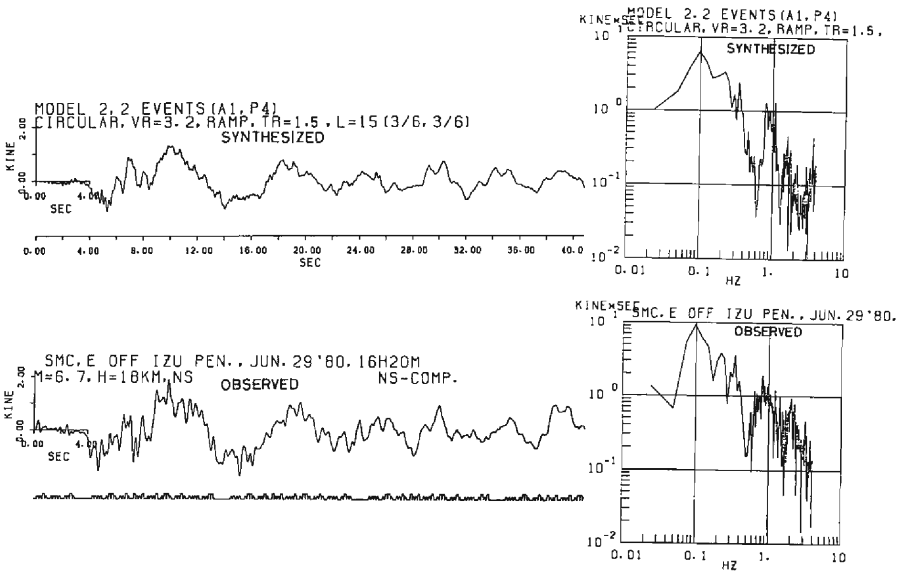

Fig. 26. Comparison of the synthesized velocity seismogram taking $\tau=1.5$ sec with the observed one for the mainshock at SMC.

function between the two seismogram because of the saturated form of the observed seismogram).

The results, showing a discrepancy between the optimum values of the rise time for the three stations, correspond to difficulties of unique determination for the rise time from seismic observations as mentioned above. For far-field observations, especially, the information on the rise time which control the short period motions seems to become more ambiguous with distance for attenuation and scattering in propagation medium. We can not discuss further which value is more probable only from this information. The rise time of 1 sec here is adopted as the optimum, determined from the data for JIZ at relatively short distance, since we have one purpose of predicting strong earthquake motions in near field.

In the synthesis done so far, we have given constraints on the mainshock rise-time and the elementary earthquake rise-time from the similarity condition (4). It is reported in some papers that the stress drops during aftershocks are not always consistent with the stress drop during the mainshock and then the similarity condition based on a constant slip velocity is not always valid, as indicated by e.g. Imagawa and Mikumo (1982). The following examination is made, to check the validity of the similarity condition (4) for the 1980 Izu-Hanto-Toho-Oki earthquakes. We synthesize the mainshock motions, assuming that the similarity conditions $L/L_e=W/W_e=D/D_e$ are valid but the slip velocity is not constant, i.e., $D/D_e\neq\tau/\tau_e$. Then the mainshock dislocation function is related to an elementary earthquake one as follows:

$$\Delta U(\xi,\eta,t)=\frac{N}{n}\sum_{k=1}^{n}\Delta U_e[\xi,\eta,t-(k-1)\tau/n]$$

where N is scaling parameter. τ_e is equal to τ for $n=1$, $\tau/2$ for $n=2, \ldots,$ and τ/N for $n=N$. The apparent oscillatory motions in this synthesis as described in the next section are reduced by the smoothing operation and filtering for the period range lower than 4 Hz. When τ_e varies τ to τ/N, i.e. $n=1$, 2, 3, 4, and N for a fixed value of $\tau=1$ sec, the coincidence between the synthesized and the observed is examined in **Fig. 27.** The best fit is obtained for $\tau_e=\tau/N$. This relation is consistent with the similarity condition, $D/D_e=\tau/\tau_e$. We compare the two synthesized seismograms, one is based on $\tau_e=\tau$ and the other, based on $\tau_e=\tau/N$, with the observed seismograms in **Fig. 28.** The synthesized seismogram for $\tau_e=\tau$ has larger amplitudes at high frequencies than that for $\tau_e=\tau/N$. The overall waveforms clearly show better fit for $\tau_e=\tau/N$.

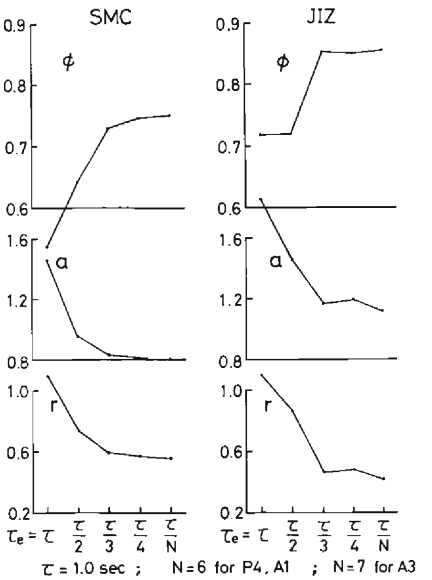

Fig. 27. The examination of the variation of the synthesized seismogram due to the relations between the rise time of the elementary earthquake and that of the mainshock, $\tau_e=\tau$, $\tau/2$, $\tau/3$, $\tau/4$, τ/N ($N=6$, for A1 and P4, $N=7$, for A3).

As the result mentioned above, we show the synthesized seismograms of NS, EW and V components for the optimum parameters at the SMC and JIZ station in **Fig. 29** and **30.** It is to be emphasized here that the synthesized seismograms are in very good agreement with the observed records for all the three components at

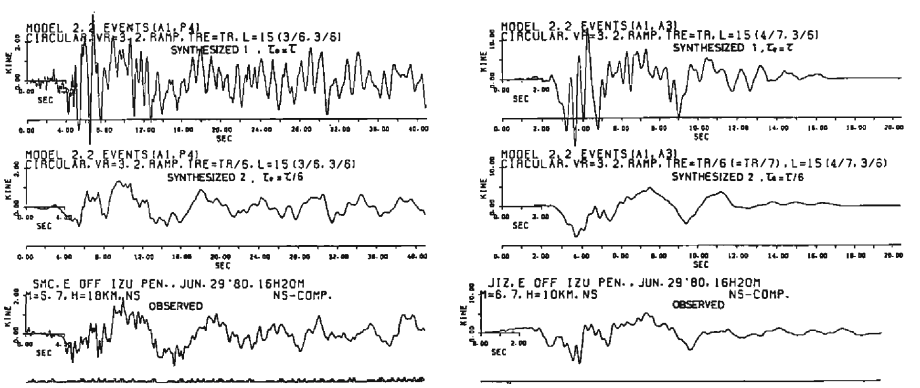

Fig. 28. Comparisons between the velocity seismograms synthesized for $\tau_e=\tau$ and for $\tau_e=\tau/6$ and the observed seismogram. (a) The case for the SMC station. (b) The case for the JIZ station.

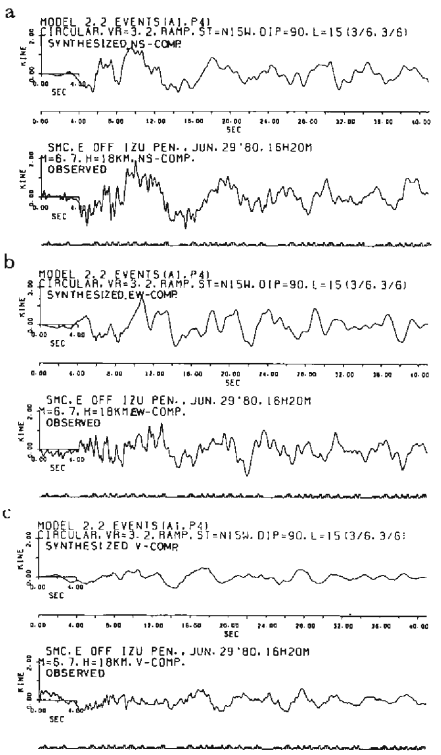

Fig. 29. Comparison of the three-components velocity seismograms(NS, EW and V) synthesized using the optimum parameters with the observed seismogram at the SMC station. (a) The case of NS-component. (b) The case of EW-component. (c) The case of V-component.

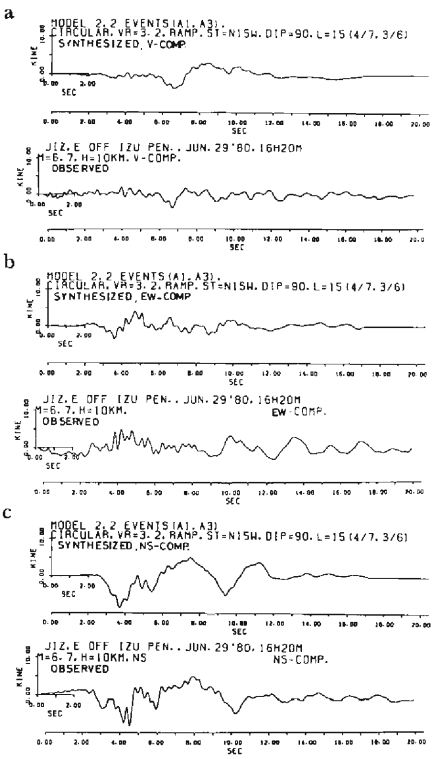

Fig. 30. Comparison of the three-components velocity seismograms(NS, EW and V) synthesized using the optimum parameters with the observed seismogram at the JIZ station. (a) The case of NS-component. (b) The case of EW-component. (c) The case of V-component.

the both stations.

4. Synthesis of Strong Acceleration Motion

4.1. Improvement (1): Removal of Ghostly Oscillatory Motion

We have so far described the synthesis of velocity seismograms and our attention was focused on frequency components lower than 1 Hz. However, ground motions with frequencies higher than 1 Hz play an important role in acceleration seismograms. We need to estimate the high frequency contents of strong motions, especially for engineering interest. The synthesized accelerogram for the mainshock can be obtained, if the accelerograms for the elementary earthquakes are put into $G_e(\boldsymbol{x}, t)$ in (22). However, we have some problems in applying (22) directly to the synthesis

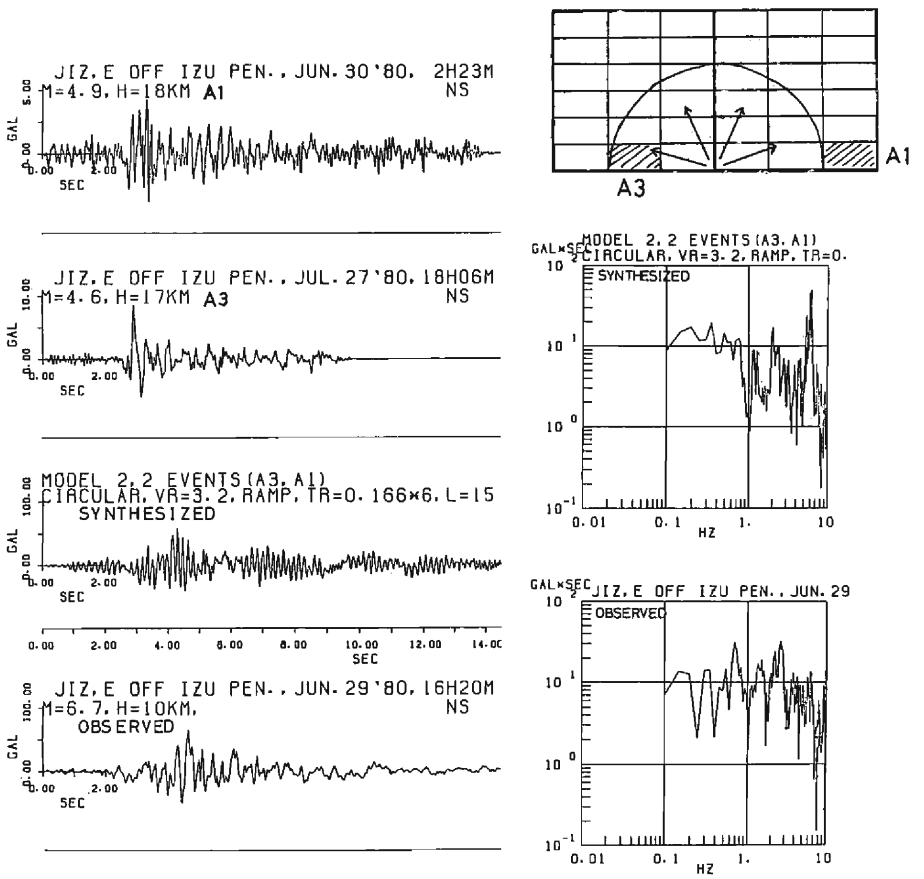

Fig. 31. Comparison of the acceleration seismogram synthesized by (22) with the observed seismogram at the JIZ station. The left upper two traces are the observed accelerograms of aftershock A1 and A3 used as elementary shocks, and the left third trace, the synthesized accelerogram for the mainshock, and the left bottom trace, the observed accelerogram of the mainshock. The right upper: the schematic mainshock fault and the elementary earthquake subfaults used for synthesis. The right middle and bottom: the Fourier sperctrum of the synthesized accelerograms and that of the observed accelerogram for the mainshock.

of the accelerogram.

One is a problem generating an apparent predominant-frequency in the synthesis following (22). The waveform and spectrum of the synthesized accelerogram for the JIZ station are compared with those of the observed one in **Fig. 31.** The waveform of the synthesized one is similar in its envelope with that of the observed one, but the two spectra are significantly different from each other in the high frequency contents. In particular, the synthesized accelerogram involves predominant frequencies around 6~7 Hz, while the observed one does not. These ghostly oscillatory motions appearing in the synthesized one are owing to the

following reasons.

The synthesized seismogram expressed by (22) is rewritten by the convolution of an elementary seismogram with a discrete time series $f(t)$,

$$f(t)=\sum_{l=1}^{N}\sum_{m=1}^{N}\sum_{k=1}^{N}\left(\frac{c_e}{c_{lm}}\right)\delta(t-t_{rlm}-(k-1)\tau_e] \tag{24}$$

where δ is the Dirac delta function. The above parameters c_e, c_{lm} and t_{rlm} are employed here to simplify the expression. That is, the mainshock motion $G(t)$ is given as

$$G(t)=f(t)*G_e(t).$$

The discrete function $f(t)$ has an apparent periodicity τ_e, as is obvious from an inspection. This periodicity is owing to (9), in which the dislocation time function of the mainshock, $\Delta U(t)$, is given by the phase delayed summation, with a constant time shift τ_e, of that of an elementary earthquake, $\Delta U_e(t)$. If both $\Delta U(t)$ and $\Delta U_e(t)$ are exact ramp functions and τ is equal to $N\cdot\tau_e$, the relation (9) is exact and then the periodicity of τ_e would not appear in the synthesized motions. This is illustrated in **Figs. 32a** and **32b**. However, the above-mentioned conditions are

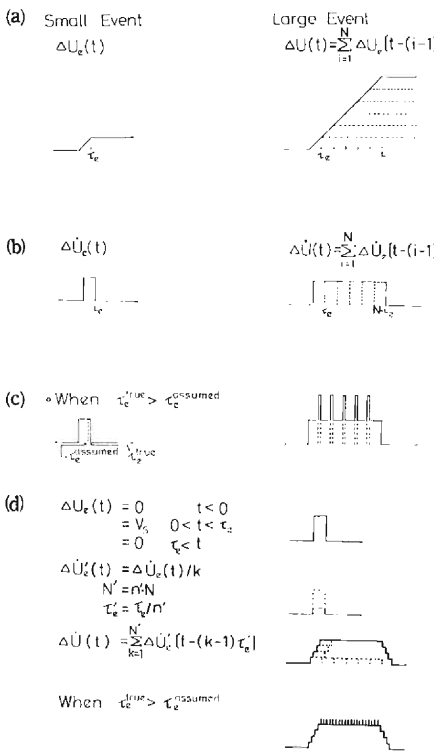

Fig. 32. (a) The dislocation time function of the small event and that of the large event, assumed to be a ramp function and $\tau_e=\tau/N$.
(b) The time derivative of the dislocation function of the small event and that of the large event.
(c) When an assumed τ_e is different from a true τ_e, the synthesized dislocation of the large event results to have an apparent periodicity at τ_e.
(d) When the operation by (22′) is made, the synthesized dislocation function is smoothed as illustrated.

unrealistic for actual synthetic problems. Even if the relation (9) is exact, it is very difficult to estimate the true value of τ_e. When the estimated value of τ_e is different from the true value, the synthesized dislocation function has an apparent predominant frequency as shown in **Fig. 32c**. When the relation (9) is not exact but holds approximately, similar oscillations are generated in the synthesis. This is the reason why the synthesized accelerogram in **Fig. 31** has ghostly predominant frequencies. Since τ_e of A1 and that of A3 has been taken to be 1/6 sec and 1/7 sec, respectively, the synthesized one has apparent predominant frequencies around 6—7 Hz.

We can avoid this difficulty by changing (22) to the following form:

$$G(t)=\sum_{l=1}^{N}\sum_{m=1}^{N}\sum_{k=1}^{N\times n'}\left(\frac{c_e}{c_{lm}}\right)\frac{1}{n'}\,G_e\left[t-t_{r_{lm}}-(k-1)\frac{\tau_e}{n'}\right] \tag{22'}$$

The meaning of this operation is a kind of smoothing as illustrated in **Fig. 32d.**

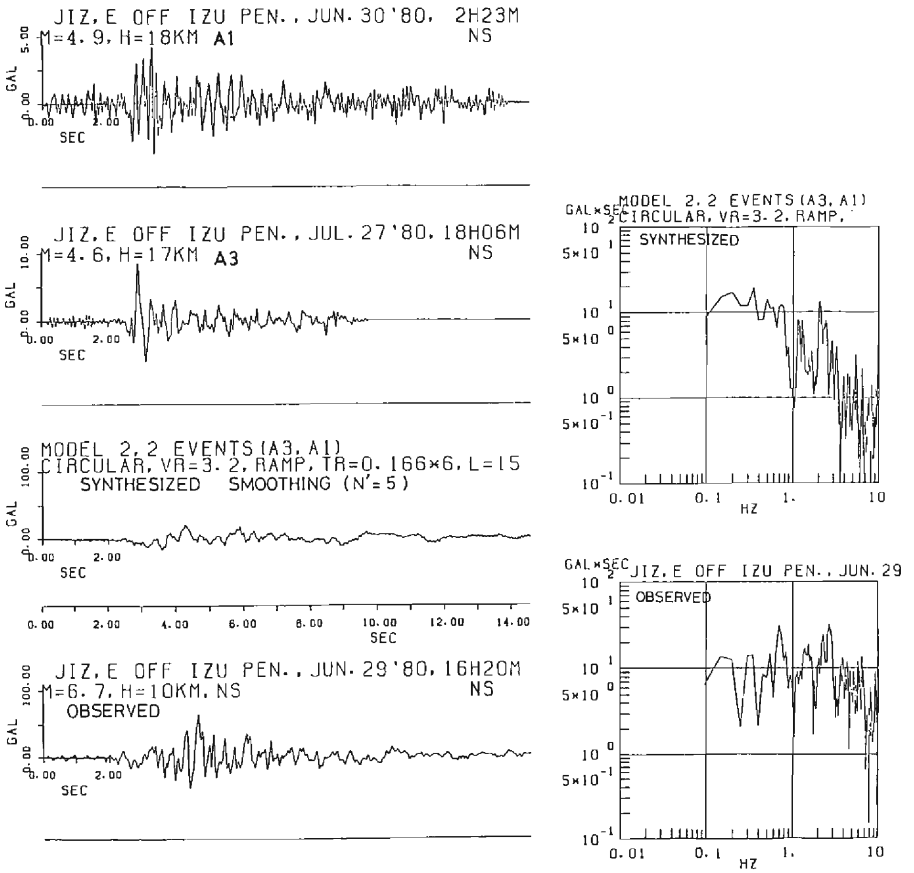

Fig. 33. Comparison of the synthesized acceleration seismogram smoothed by (22') with the observed seismogram at the JIZ station.

Applying (22′) to the synthesis, the apparent periodicity is shifted to the shorter period, τ_e/n'. Then we can obtain the synthesized motions up to the frequency range of engineering interest.

Applying the revised formulation (22) with $N'=5$, we make a synthesis for the mainshock accelerogram at JIZ. The waveform and the spectrum of the synthesized seismogram are shown in **Fig. 33,** after low-pass-filtering with a 10 Hz cut-off frequency. The ghostly oscillatory motions owing to τ_e disappear in the synthesized seismogram. However, the synthesized one has significantly small amplitudes for the frequency range higher than 1 Hz, compared with the observed one. This is discussed in the next section.

4.2. Improvement (2); Revised Synthesis Method for High-Frequency Motion.

Our synthesis formulation (19) is based on the representation of the source time function in the far-field due to a constant dislocation over a fault plane in an infinite homogeneous elastic medium, i.e. (6). When a coherent rupture propagation and a constant dislocation represented by a linear ramp time function are assumed over a rectangular fault plane, the source time function expressed by (6) has flat spectra at low frequencies and ω^{-3} high-frequency asymptotes. For the case of Model H1-1 in section 2.4, the spectral amplitude of the source time function can be obtained in the simple expression (Mikumo, 1971[35] and Geller, 1976[27]):

$$|S(\omega)|=\mu\left|\frac{\sin(\omega X_\tau)}{\omega X_\tau}\right|\cdot\left|\frac{\sin(\omega X_L)}{\omega X_L}\right|\cdot\left|\frac{\sin(\omega X_W)}{\omega X_W}\right| \tag{25}$$

where $X_L=|L(1/v_R-\cos\varphi/v_c)/2|$, $X_W=|W\cos\theta\sin\varphi/(2v_c)|$ and $X_\tau=\tau/2$. It is clear from (25) that the source time function of Models H1-1 and H1-2 have ω^{-3} decay at the high frequencies. Similarly, for the case of Model H2-2 the source time function has a flat spectrum at low frequencies and ω^{-3} decay usually at the frequencies higher than $1/\tau$, as shown in **Fig. 9,** although the Fourier spectrum can not be obtained in an analytical expression.

Thus, in our synthesis formultion, the spectrum of $G(x, t)$ expressed by a triple integral such as (19) yields ω^{-3} decay at frequencies higher than $1/\tau$, if $G_{elm}(x, t)$ has a flat spectrum. The synthesized seismogram shown in **Fig. 31** has smaller amplitudes than the observed one at frequencies higher than about 1 Hz (consistent with $1/\tau$). This means that there is large discrepancy between the characteristic features involved in the observed seismogram and the assumption in our synthesis in the frequency range higher than $1/\tau$. This problem is related to the basic assumption in our formulation, that is, a smooth rupture propagation over a rectangular fault plane. To recover the fall-off of the spectral amplitudes at frequencies higher than 1 Hz to the observed level, it would be necessary to introduce inhomogeneous fault models such as those including 'barriers' (e.g. Das and Aki, 1977[12]). However, from another point of view we can apply the present synthesis method to

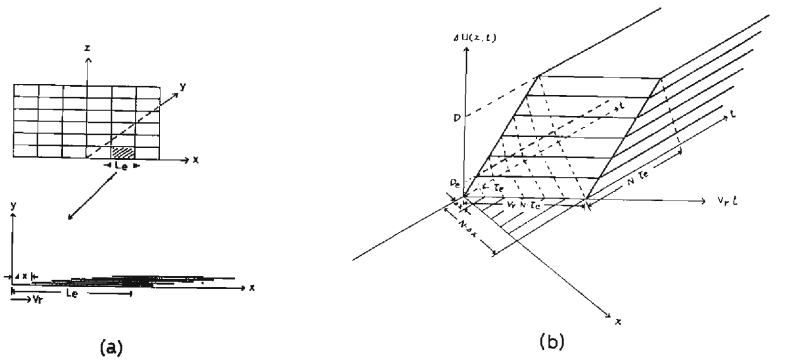

Fig. 34. (a) The distribution of subfaults during a large event. Each subfault corresponds to a small event.
(b) The relation between the dislocation time function of the small event and that of the large event in the space and time domain when is considered the distribution of subfaults as shown in (a).

estimate the high frequency motions by modifying our formulation without directly presuming 'barriers', if we use elementary earthquakes having a characteristic scale involved in the mainshock phenomena.

Now, we return this discussion to the relation (9),

$$\Delta U(\xi, \eta, t) = \sum_{k=1}^{N_D} \Delta U_e[\xi, \eta, t-(k-1)\tau_e] \qquad \text{again (9)}$$

and start to revise the formulation. In section 2.2, we introduced (9), only in the time domain, to satisfy the similarity condition,

$$D/D_e = \tau/\tau_e = N_D \tag{26}$$

The relation (9) is here reconsidered to have a physical meaning in the space and time domain during the mainshock. Suppose that N_D subfaults are aligned in a certain space interval Δx contacting one plane after another as shown in **Fig. 34a.** The length of a subfault corresponds to that of an elementary earthquake, L_e. Accordingly, a uniform dislocation on a subfault is taken to be consistent with the same distribution as the dislocation during an elementary earthquake. Then the dislocation during the mainshock is expressed by the delayed summation of the dislocation during the elementary earthquake along the x-axis,

$$\Delta U(x) = \sum_{k=1}^{N_D} \Delta U_e[x-(k-1)\Delta x]. \tag{27}$$

When the rupture of the subfaults propagates along the positive direction of the x-axis with the velocity v_r, (27) can be rewritten in time domain,

$$\Delta U(t) = \sum_{k=1}^{N_D} \Delta U_e\left[t-(k-1)\frac{\Delta x}{v_r}\right] \tag{28}$$

If Δx is replaced by $v_r \cdot \tau_e$, equation (28) becomes equivalent to (9). Thus, we can rewrite the relation (9) by presuming the space and time distribution of the subfaults as shown in **Fig. 34b** as follows:

$$\Delta U(\xi, \eta, t) = \sum_{k=1}^{N_D} \Delta U_e[\xi - (k-1)v_r\tau_e, \eta, t], \tag{29a}$$

and

$$\Delta U(\xi, \eta, t) = \sum_{k=1}^{N_D} \Delta U_e[\xi, \eta - (k-1)v_r\tau_e, t]. \tag{29b}$$

Since ξ and η are taken along the strike and the dip directions, respectively, (29a) is an intuitively clear relation to express the case of strike-slip type fault, while (29b) is suitable for the case of the dip-slip type fault.

We have adopted (29a) in this study, since the 1980 Izu-Hanto-Toho-Oki earthquake we have analyzed here has the strike-slip type mechanism. Consequently, equations (19) and (20) are rewritten as follows:

$$G(x, t) = \sum_{k=1}^{N_D} \sum_{l=1}^{N_L} \sum_{m=1}^{N_W} G_{elm}(x, t - t'_{dklm}) \tag{30}$$

$$t'_{dklm} = \frac{r_{lm}}{v_c} + \frac{\sqrt{[\xi_l \mp (k-1)\Delta x_e]^2 + \eta_m^2}}{v_r} \tag{31}$$

$$\Delta x_e = v_r \tau_e \tag{32}$$

If we use elementary earthquakes with the fault length $L_e = N_D \Delta x_e$ for the synthesis, (30) and (31) are further rewritten.

$$G(x, t) = \sum_{l'=1}^{N_D \times N_L} \sum_{m=1}^{N_W} G_{elm}(x, t - t'_{dl'm}) \tag{30'}$$

$$t'_{dl'm} = \frac{r_{l'm}}{v_c} + \frac{\sqrt{\xi_{l'}^2 + \eta_m^2}}{v_r} \tag{31'}$$

where

$$\eta_m = (m-1)W_e, \ m = 1, 2, \ldots, N_W,$$
$$\xi_{l'} = (l'-1)L_e/N_D, \ l' = 1, 2, \ldots, N_L \times N_D,$$

and G_{elm} is a seismogram from an element $\Delta\Sigma_{lm}$ ($l = 1 \sim N_L$ and $m = 1 \sim N_W$).

The accelerogram synthesized by (30′) has ω^{-2} decay when each G_{elm} has an flat spectrum so that it has more rich high-frequency motions than that synthesized by (19). This tends to reduce the above-described discrepancy between the synthesized and the observed accelerograms. The synthesis by (30′) need not apparently give both the rise time τ for the mainshock and τ_e for elementary earthquakes. Actually, we have to use elementary earthquakes with a definite fault length, $L_e = N_D \Delta x_e = v_r \cdot N_D \tau_e = v_r \cdot \tau$. Since $\tau \approx 1$ sec and $v_r \approx 3$ km/sec for 1980 Izu-Hanto-Toho-Oki, we need to use foreshocks or aftershocks with the length of about 3 km.

Bouchon (1978)[36] showed that the multiple cracks with barriers are roughly equivalent to dislocation model with a uniform slip of the Haskell-type source. Based on this evidence, Aki et al. (1977)[37] showed that one can make a rough estimate of a barrier interval from the rise time in such a way that

$$\text{(barrier interval)} \sim \text{(rupture velocity)} \cdot \text{(rise time)} \tag{33}$$

On the other hand, Aki et al. summarized probable barrier intervals inferred from the observed fault slip for several earthquakes studied by Matsuda (1972[38] and others). They inferred an average barrier interval of 3 km for the 1974 Izu-Hanto-Oki earthquake based on Matsuda and Yamashina (1974)[39]. It is of interest that 'barrier interval' from (33) is about 3 km for the 1980 Izu-Hanto-Toho-Oki earthquake and almost the same as that for the 1974 Izu-Hanto-Oki Earthquake which occurred in the near region southwest of the 1980 Izu-Hanto-Toho-Oki earthquake.

It is concluded from the revised formulation (30′) that for the synthesis of high frequency motions it would be better to use elementary earthquakes with the characteristic scale of the fault length,

(fault length of elementary earthquake)∼(rise time of the mainshock) · (rupture velocity).

Under this condition, the synthesized motions do not miss the high frequency constituents including the source characteristics of the elementary earthquakes. According to the 'barrier model', this means that the optimum elementary earthquakes for the synthesis should have a fault length consistent with a 'barrier interval' of the mainshock.

4.3. Synthesized Results of Strong Accelerograms Using the Revised Method

The fault lengths of foreshock P4 and aftershock A1 with $M=4.9$ are estimated to be both about 2.5 km from the similarity condition $L_e/L=\sqrt[3]{Mo/Mo_e}=N$, where N is estimated to be about 6 from the spectral ratios between the mainshock and the small events as discussed in section 3.2. and L is estimated to be 15 km from the epicentral distribution of the aftershocks. Similarly, the fault length of aftershock A3 with $M=4.6$ is estimated as about 2.1 km. In order to make a synthesis by the revised formulation (30′), it is necessary to use the records from elementary earthquakes having the fault length of about 3 km from the condition $L_e=v_r\cdot\tau$. The three events P4, A1 and A3 are regarded as having the fault length of the same order. Therefore, using the observed seismograms from these events, we make a synthesis of the mainshock motions by means of (30′). An operation of smoothing has been made on the basis of (22′), to reduce the ghostly oscillatory motions due to the apparent periodicity of $\Delta x/v_r$ corresponding to τ_e mentioned in section 4.1.

The waveform and the spectrum of NS-component of the synthesized seismogram for the JIZ station are compared with those of the observed one in **Fig. 35.** The upper two traces are the observed seismograms from events A1 and A3 used as

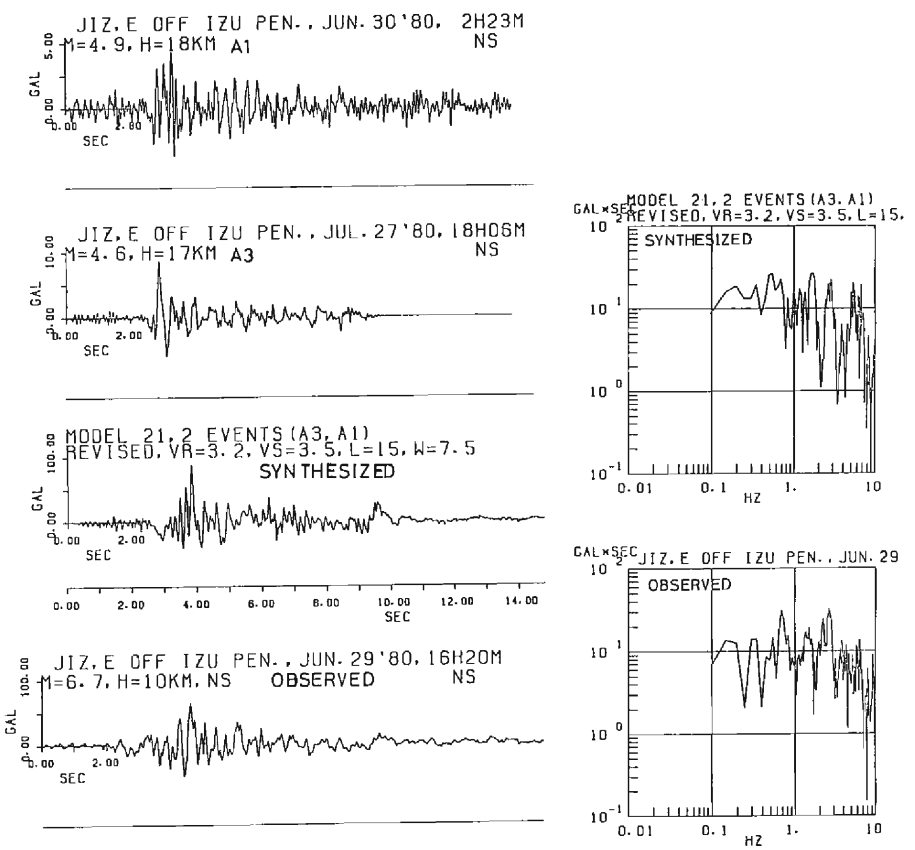

Fig. 35. Comparison of the synthesized acceleration seismogram of NS component by the revised formulation (30′) with the observed seismogram at the JIZ station. The left upper two traces are the observed accelerograms of aftershock A1 and A3 used as elementary earthquakes, the left third trace, the synthesized accelerogram and the left bottom trace, the observed accelerogram of the mainshock. The right upper figure is the Fourier spectrum of the synthesized accelerogram and the lower figure, that of the observed mainshock one.

the elementary earthquakes. The parameters, except for τ_e, are given to be the same values as the case of the synthesized velocity motions in section 3.3. It is not neccessary to give τ_e but to give $\Delta x = L_e/N$. The third and the fourth trace in **Fig. 35** show the synthesized and the observed accelerogram. The envelope of the synthesized waveform agree well with that of the observed one, although the two waveforms do not always correspond to each other in individual phases. The spectral amplitudes of the synthesized accelerogram (the right upper figure in **Fig. 35**) agree well with those of the observed one (the right lower figure) at the frequencies up to 5 Hz.

The waveform and the spectrum of NS-component of the synthesized accelerogram for the SMC station are compared with those of the observed one in **Fig. 36.**

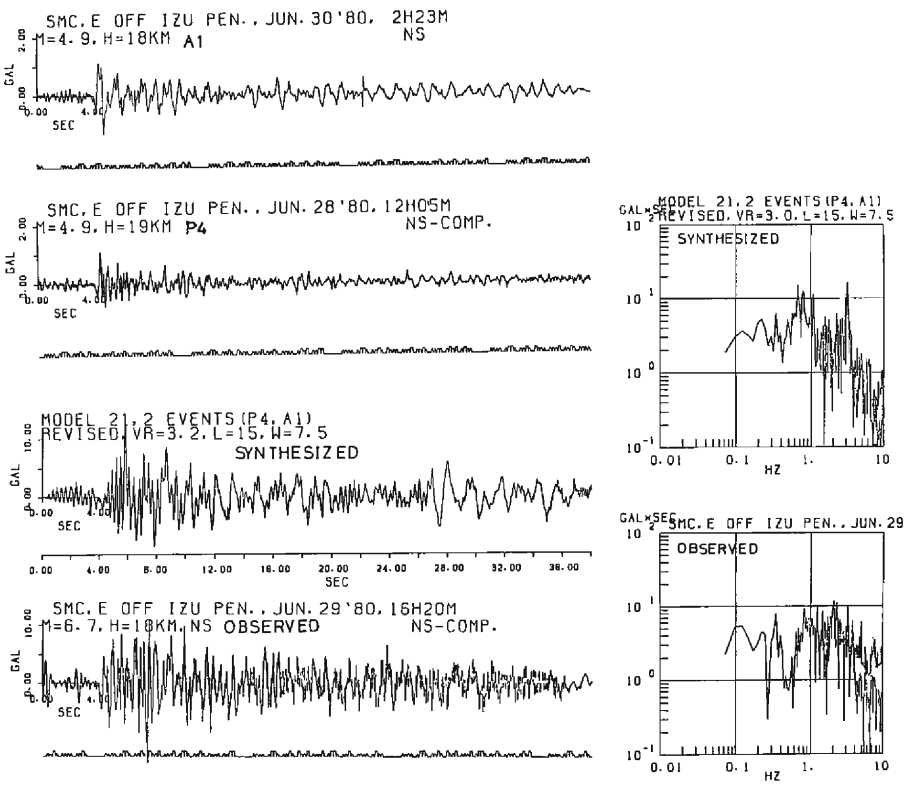

Fig. 36. Comparison of the synthesized acceleration seismogram of NS-component by the revised formulation (30′) with the observed seismogram at the SMC station. The arrangement of the figures is the same as Fig. 33.

The two events P4 and A1 are used as the elementary earthquakes for the present synthesis. Similar to the case of the JIZ station, the parameters are given to be the same as the case of the synthesized velocity motions. The envelope of the synthesized waveform also agrees well with that of the observed one. As compared in the right figures, the spectral amplitudes of the synthesized one agree well with those of the observed one at the frequencies up to 5 Hz, similar to the case of the JIZ station.

Fig. 37 shows the V-component seismograms of the synthesized acceleration motions and the observed ones for JIZ station and SMC station. We can see the vertical component synthesized-accelerograms are also in a good agreement in its envelope with the observed ones for the both stations.

These results show that the revised method (30′) is extremely useful for the synthesis of high frequency motions up to 5 Hz. We consider that it is difficult to synthesize deterministically higher frequency motions beyond 5 Hz, because these high-frequency motions may be represented as having statistical natures in source effect and path effect as discussed by Andrews (1981)[40] and others.

The frequency range effective for the synthesis by the revised method (30′)

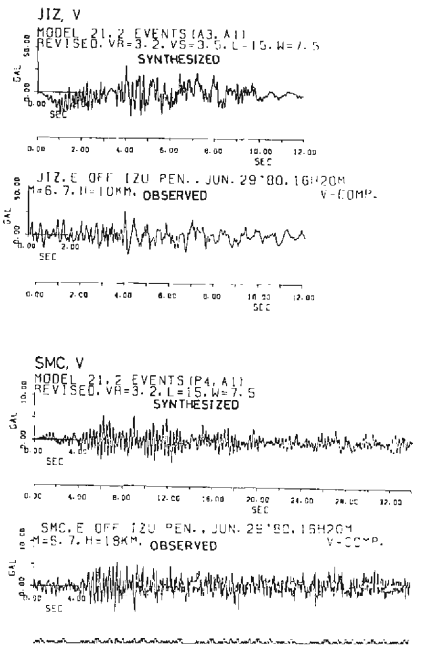

Fig. 37. Comparison of the synthesized acceleration seismograms of V-component by the revised formulation (30′) with the observed seismograms at the JIZ and SMC station.

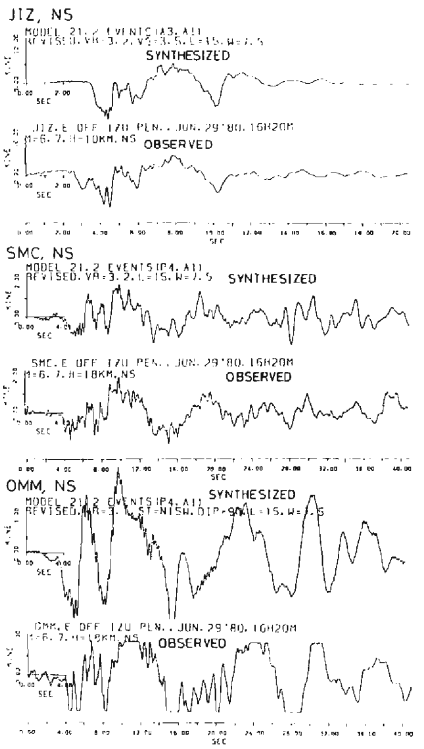

Fig. 38. Comparison of the synthesized velocity seismograms of NS-component by the revised formulation (30′) with the observed seismograms at the JIZ, SMC and OMM station.

is not restricted to high frequencies. By means of this revised method the synthesized velocity motions for the JIZ, SMC and OMM station are compared with the observed ones in **Fig. 38.** We can see an extremely good agreement between the synthesized and the observed seismograms for the three stations.

This revised formulation is also based on a smooth rupture propagation over a fault plane. However, seismic effects due to the complex nature of the rupture process inside the blocks with the length L_e, corresponding to the source sizes of small events, are kept in the synthesized results without being filtered in time domain through the synthesis procedure. This formulation is based on an idea that the similarity condition between the dislocation of the mainshock and that of small events is satisfied in each block with the length $v_r \cdot \tau$. If the length of each block is regarded as a kind of barrier interval, this synthesis method is interpreted to be close to computational models of multiple cracks with barriers shown by Bouchon (1978)[36] and Madariaga (1974)[41].

5. Conclusion

1. The synthesis method described in this paper is based on the representation, including the source effects, relating to the dislocation at every point on the fault plane and to the rupture propagation over the fault plane, and the path effects, relating to the wave propagation from the source to the site, although some approximations are made. If there is a certain similarity relation between large earthquakes and small ones within the same source area, the equation for the synthesis is an accurate approximation for the wave field from the source to the site.
2. The synthesis method is checked by synthesizing the velocity motions of the mainshock for 3 stations at the short distances (Δ=20—100 km) from the epicenter in the case of the 1980 Izu-Hanto-Toho-Oki earthquake, using the records of two small events, whose hypocenters are located at the northern half area and the southern half area of the mainshock fault plane, respectively. The synthesized seismograms show a good agreement with the observed seismograms in the frequency range less than 1 Hz.
3. The validity of the assumed source parameters, such as the starting point of rupture, the rupture velocity, and the rise time is examined by means of three kinds of measure, a correlation function, an amplitude ratio and a residual function between the synthesized seismograms and the observed seismograms of the mainshock. We find that the best agreement between the two seismograms is obtained for the model expected from the epicentral and depth distribution of the aftershocks and the similarity condition between the mainshock and the small events. These results show that the present synthesis is physically meaningful.
4. A synthesis method for higher frequency motions is further revised by changing the relation in the time domain between the dislocation function of the mainshock and that of small events to the relation in time-space domain between them. When we use the records from the small events having the fault length $L_e=v_r\cdot\tau$ (v_r: the rupture velocity, τ: the rise time of the mainshock), this revised synthesis is effective for higher frequency motions. The synthesized accelerograms by this revised method show a good agreement with the observed accelerograms of the mainshock in the frequency range up to 5 Hz.

Acknowledgements

The author is grateful to Prof. S. Yoshikawa for critically reading to improve this paper and for his encouragement in carrying out this work. The author thanks Prof. I. Muramatu for his valuable suggestions and comments. The observation for this study was performed in collaboration with him. The author has benefitted greatly from discussion of Prof. T. Mikumo and the motivation of this study arose from his suggestions. The authour thanks Prof. Y. Kobayashi for many stimulating discussions and comments. Dr. Kinoshita kindly provided the digital data obtained

at the Nakaizu station (JIZ) of National Research Center for Disaster Prevention, the Science and Technology Agency. Helpful discussions during the course of this work with Mr. M. Horike, F. Amaike, S. Kasuga and many other colleagues are also gratefully acknowledged. The author thanks also to Mr. M. Nishi for his co-operation in the observation and Mrs. K. Kutsuki for arranging this paper. The author would like to acknowledge an anonymous reviewer for very careful help to improve the manuscript. This research was supported in part by a Grant-in-Aid for Natural Disaster Scientific Research from the Ministry of Education, Science and Culture under Grant No. 57025025. The data processing was run on a Facom M-140 at the Information Data Processing Center for Disaster Prevention Research, of Disaster Prevention Research Institute of Kyoto University.

References

1) Aki, K.: Seismic Displacements near a Fault, J. Geophys. Res., Vol. 73, 1968, pp. 5359–5376.
2) Haskell, N. A.: Elastic Displacements in the Near-Field of a Propagating Fault, Bull. Seism. Soc. Am., Vol. 59, 1969, pp. 865–908.
3) Kawasaki, I., Y. Suzuki, and R. Sato: Seismic Waves Due to a Shear Fault in a Semi-infinite Medium, J. Phys. Earth, Vol. 21, 1973, pp. 251–254.
4) Sato, R.: Long-Period Surface Velocities and Accelerations Due to a Dislocation Source Model in a Medium with Spherical Multi-Layers, Part II, J. Phys. Earth, Vol. 26, 1978, pp. 17–37.
5) Sato, R. and N. Hirata: One Method to Compute Theoretical Seismogram in a Layered Medium, J. Phys. Earth, vol. 28, 1980, pp. 145–168.
6) Heaton, T. H. and D. V. Helmberger: Generalized Ray Models of the San Fernando Earthquakes, Vol. 67, 1979, pp. 1311–1341.
7) Bouchon, M.: Discrete Wave Number Representation of Elastic Wave Fields in Three-Space Dimensions, J. Geophys. Res., Vol. 84, 1979, pp. 3609–3614.
8) Hartzell, S. and D. V. Helmberger: Strong Motion Modeling of the Imperial Valley Earthquake of 1979, Bull. Seism. Soc. Am., Vol. 72, 1982, pp. 571–596.
9) Alekseev, A. S. and B. G. Mikhailenko: Numerical Modelling of Transient Wave Fields in Seismology and Seismic Prospecting, Siberian Branch of Academy of Sciences of the USSR, Novosibirsk. 1979.
10) Aki, K.: Characterization of Barriers on an Earthquake Fault, J. Geophys. Res., Vol. 84, 1979, pp. 6140–6148.
11) Mcgarr, A.: Analysis of Peak Ground Motion in Terms of a Model of Inhomogeneous Faulting, J. Geophys. Res., Vol. 86, 1981, pp. 3901–3902.
12) Das, S. and K. Aki: Fault Plane with Barriers: A Versatile Earthquake Model, J. Geophys. Res. 82, 1977, pp. 5648–5670.
13) Mikumo, T. and T. Miyatake: Dynamical Rupture Process on a Three-Dimensional Fault with Non-Uniform Frictions and Near-Field Seismic Waves, Geophys. J. Roy. Astron. Soc., Vol. 54, 1978, pp. 417–438.
14) Papageorgiou, A. S. and K. Aki: A Specific Barrier Model for the Quantitative Description of Inhomogeneous Faulting and the Prediction of Strong Ground Motion, I and II, in Proceedings of Workshop XVI—The Dynamic Characteristics of Faulting Inferred from Recordings of Strong Ground Motion, Vol. 1, J. Boatwright, Editor, U.S. Geol. Surv., Open-File Rept. 82–591, 1982, pp. 311–504.
15) Boatwright, J.: A Dynamic Model for Far-Field Acceleration, Bull. Seism. Soc. Am., Vol. 72, 1982, pp. 1049–1068.
16) Madariaga, R.: High-Frequency Radiation from Crack (Stress-Drop) Models of Earthquake

Faulting, Geophys. J. Roy. Astron. Soc., Vol. 51, 1977, pp. 625–652.
17) Hartzell, S.: Earthquake Aftershocks as Green's Functions, Geophys. Res. Letters, Vol. 5, 1978, pp. 1–4.
18) Kanamori, H.: A Semi-Empirical Approach to Prediction of Long-Period Ground Motions from Great Earthquakes, Bull. Seism. Soc. Am., Vol. 69, 1979, pp. 1654–1670.
19) Hadley, D. M. and D. V. Helmberger: Simulation of Strong Ground Motions, Bull. Seism. Soc. Am., Vol. 70, 1980, pp. 617–630.
20) Irikura, K. and I. Muramatu: Synthesis of Strong Ground Motions from Large Earthquakes Using Observed Seismograms of Small Events, Proceedings Third International Earthq. Microzonation Conf., Seattle, Vol. 1, 1982, pp. 447–458.
21) Imagawa, K. and T. Mikumo: Near-Field Seismic Waveforms from Major Earthquakes and Consideration on the Rupture Process on the Fault, Jishin, Vol. 35, 1982, pp. 575–590 (in Japanese).
22) Iida, M. and M. Hakuno: Estimation of Building Response Due to Large-scale Earthquake from Observed Response Records to Small Earthquakes, Proceedings Third International Earthq. Microzonation Conf., Seattle, Vol. 11, 1982, pp. 895–908.
23) Aki, K.: Scaling Law of Seismic Spectrum, J. Geophys. Res., Vol. 72, 1967, pp. 1217–1231.
24) Aki, K.: Scaling Law of Earthquake Source Time-Function. Geophys. J. R. Astron. Soc., 31: 3–25, 1972.
25) Kanamori, H. and D. L. Anderson: Theoretical Basis of Some Empirical Relations in Seismology, Bull. Seism. Soc. Am., Vol. 65, 1975, pp. 1073–1095.
26) Tsuboi, C.: Earthquake Energy, Earthquake Volume, Aftershock Area and Strength of the Earth's Crust, J. Phys. Earth, Vol. 4, 1956, pp. 63–66.
27) Geller, R. J.: Scaling Relations for Earthquake Source Parameters and Magnitudes, Bull. Seism. Soc. Am. Vol. 66, 1976, pp. 1501–1523.
28) Abe, K.: Reliable Estimation of the Seismic Moment of Large Earthquakes, J. Phys. Earth, Vol. 23, 1975, pp. 381–390.
29) Haskell, N. A.: Radiation Pattern of Surface Waves from Point Source in a Multi-Layered Medium, Bull. Seism. Soc. Am., Vol. 54, 1964, pp. 377–393.
30) Aki, K., and P. G. Richard: Quantitative Seismology, Theory and Method, Vol. 2, Chapter 14, pp. 804–805, W. H. Freman and Company, 1980.
31) Chouet, B., K. Aki and M. Tsujiura: Regional Variation of the Scalling Law of Earthquakes Source Spectra, Bull. Seism. Soc. Am., Vol. 68, 1978, pp. 49–79.
32) Muramatu, I.: A Velocity Type Strong Motion Seismograph with Wide Frequency Range, J. Seism. Soc. Japan, JISHIN, Vol. 30, 1977, pp. 317–338 (in Japanese).
33) Kinoshita, S.: Parallel Observation of Strong Ground Motion by Using Both Acceleration and Velocity Type Seismometers at Nakaizu Crustal Active Observatory, Research Notes National Res. Center Disast. Prev., Vol. 44, 1981, pp. 1–31.
34) Imoto, M., I. Karakama, R. S. Matsuura, F. Yamazaki, A. Yoshida and K. Ishibashi: Focal Meshanisms of the 1980 Earthquake Swarm off the East Coast of the Izu Peninsula, Japan, JISHIN, Vol. 34, 1981, pp. 481–493.
35) Mikumo, T.: Source Process of Deep and Intermediate Earthquakes as Inferred from Long-Period P and S Waveforms, J. Phys. Earth. Vol. 19, 1971, pp. 1–20.
36) Bouchon, M.: A Dynamic Source Model for the San Fernando Earthquake, Bull. Seism. Soc. Am., Vol. 68, 1978, pp. 1555–1576.
37) Aki, K., M. Bouchon, B. Chouet, and S. Das: Quantitative Prediction of Strong Motion for a Potential Earthquake Fault, Annali di Geogisica, Vol. 30, 1977, pp. 341–368.
38) Matsuda, T.: Surface Faults Associated with Kita-Izu Earthquake of 1930 in Izu Peninsula, Japan, The Izu Peninsula, deited by M. Hoshino and H. Aoki, Tokai Univ. Press, Tokyo., 1972.
39) Matsuda, T. and K. Yamashina: Surface Faults Associated with the Izu-Hanto-Oki Earthquake of 1974, Japan, Sokuho (in Japanese). Earthq. Res. Inst. Univ. Tokyo, Vol. 14, 1974,

pp. 135–158.
40) Andrews, D. J.: A Stochastic Fault Model, 2. Time-Dependent Case, J. Geophys. Res., Vol. 86, 1981, pp. 10321–10834.
41) Madariaga, R.: On the Relation between Seismic Moment and Stress Drop in the Presence of Stress and Strength Heterogeneity, J. Geophys. Res., Vol. 84, 1979, pp. 2243–2250.